Southeastern Geology: Volume 33, No. 1 October 1992

Editor in Chief: S. Duncan Heron, Jr.

Abstract

Academic journal published quarterly by the Department of Geology, Duke University.

SOUTHEASTERN GEOLOGY

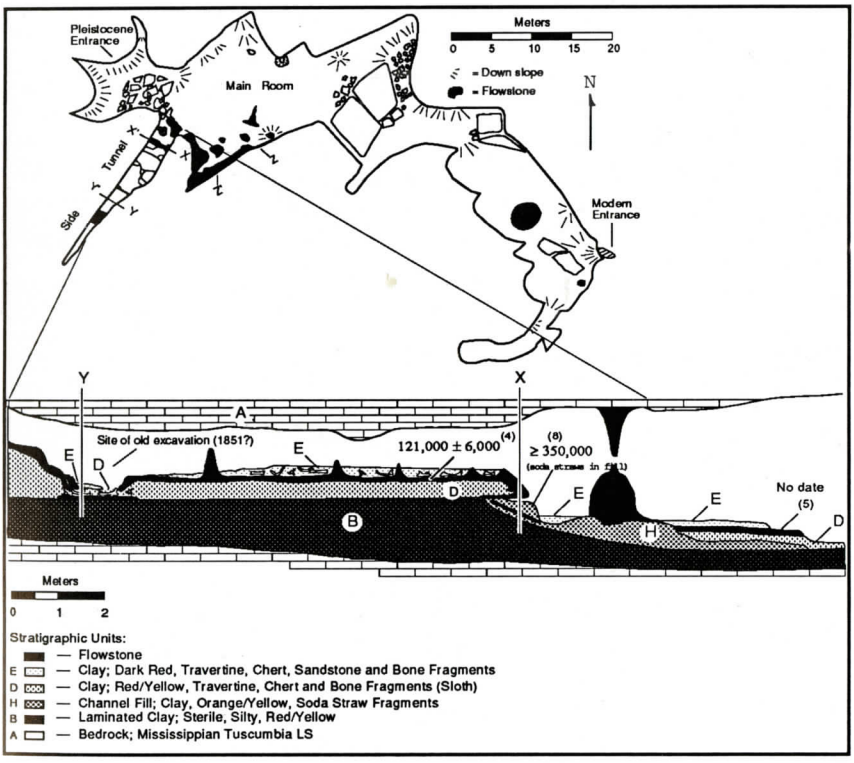

VOL. 33, NO. 1 OCTOBER 1992

SOUTHEASTERN GEOLOGY

PUBLISHED

at

DUKE UNIVERSITY

Editor in Chief:

Duncan Heron

This journal publishes the results of original research on all phases of geology, geophysics, geochemistry and environmental geology as related to the Southeast. Send manuscripts to **DUNCAN HERON, DUKE UNIVERSITY, DEPARTMENT OF GEOLOGY, BOX 90233, DURHAM, NORTH CAROLINA 27708**. Phone 919-684-5321, Fax 919-684-5833. Please observe the following:

1) Type the manuscript with double space lines and submit in duplicate.
2) Cite references and prepare bibliographic lists in accordance with the method found within the pages of this journal.
3) Submit line drawings and complex tables reduced to final publication size (no bigger than 8 x 5 3/8 inches).
4) Make certain that all photographs are sharp, clear, and of good contrast.
5) Stratigraphic terminology should abide by the North American Stratigraphic Code (American Association Petroleum Geologists Bulletin, v. 67, p. 841-875).

Subscriptions to *Southeastern Geology* per volume are: individuals - $14.00 (paid by personal check); corporations and libraries - $19.00; foreign $23. Inquires should be sent to: **SOUTHEASTERN GEOLOGY, DUKE UNIVERSITY, DEPARTMENT OF GEOLOGY, BOX 90233, DURHAM, NORTH CAROLINA 27708**. Make checks payable to: *Southeastern Geology.*

SOUTHEASTERN GEOLOGY is a peer review journal.

ISSN 0038-3678

SOUTHEASTERN GEOLOGY

Table of Contents

Vol. 33, No. 1

October 1992

SOUTHEASTERN GEOLOGY
V. 33, No. 1, October 1992, p. 1-8

URANIUM-SERIES DATES FROM TRAVERTINES ASSOCIATED WITH A LATE PLEISTOCENE MEGAFAUNA IN ACb-3, ALABAMA

R. S. LIVELY
Minnesota Geological Survey
2642 University Ave.
St. Paul, MN 55114

G. L. BELL, JR.
Dept. of Geological Sciences
University of Texas at Austin
Austin, TX 78713

J. P. LAMB, JR.
Red Mountain Museum
1421 22nd St. So.
Birmingham, AL 35205

ABSTRACT

U-series dates on flowstone interbedded with bone-bearing sediments indicate that Cave ACb-3 was accumulating small vertebrate remains as early as 228,000 years B.P. and was visited by large vertebrates from about 170,000 years to at least 115,000 years B.P. and probably later.

INTRODUCTION

Before 1976, no unequivocal Pleistocene faunas had been reported from Alabama (Kurten and Anderson, 1980). Since then, Currin and others (1976) and Womochel (1982) have described Pleistocene faunal remains discovered in fluvial sediments and in a sinkhole fill in northwestern Alabama. More recently, also in northwestern Alabama, a large faunal assemblage of sloths (*Megalonyx jeffersoni*), a sabertooth cat (*Smilodon*) and over 20 species of smaller vertebrate fauna was discovered in a cave being studied by the Red Mountain Museum, Birmingham, Alabama. This site was significant because some the bone-bearing sediments were between, or capped by, secondary deposits of calcium carbonate (flowstone) that could be dated using the U-series method (Ivanovich and Harmon, 1982). In addition, the low-energy cave environment kept the faunal remains in very good condition, unlike some surface deposits formed in high-energy fluvial systems.

Kurten and Anderson (1980), reviewing dated faunal sites younger than 350,000 years B. P., listed only one with a fairly well-constrained absolute date. Other sites referenced to that time period were based on biostratigraphic evidence. Cave ACb-3, with datable flowstone interbedded with sediments and faunal remains, is a good site at which to develop a local chronologic framework that extends beyond the range of radiocarbon dating. This paper describes the cave and the results of the U-series dating analyses. A detailed description of the fauna has not been completed.

REGIONAL GEOLOGY

Cave ACb-3 is in the Pride quadrangle, Colbert County, northwestern Alabama (Fig. 1). The area is part of the Interior Low Plateaus physiographic province (Szabo, 1975). The geology of the quadrangle consists of nearly flat (<1° dip to the southwest) Mississippian and Cretaceous sedimentary rocks and occasional Quaternary terrace deposits next to the Tennessee River.

The Mississippian section, beginning at the base, consists of the Fort Payne Chert, a thin-bedded siliceous limestone; the Tuscumbia

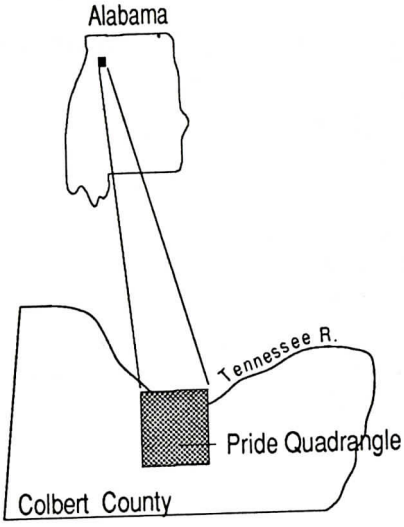

Figure 1.-Location of study area in northwestern Alabama, southeastern United States. The exact cave location is not shown.

Limestone, an interbedded limestone and shale; and interbedded sandstone, shale and limestone of the Pride Mountain Formation, the Hartselle Sandstone and the Bangor Limestone (Szabo, 1975). The Pride Mountain Formation has a dissected vertical relief of about 200 feet near the Tennessee River where it is capped by Quaternary terraces. To the south the uplands are capped by the Hartselle Sandstone and reach about 400 feet above river level.

The Tuscumbia Limestone is host to karst features consisting of sinkholes, solution-enlarged joints, and caves. Karst development appears to be at least partially controlled by existing joints in the bedrock. The principle joint system strikes to the northwest; a secondary joint set strikes to the northeast. Cave chamber orientation appears to follow the northeast trend, although other karst features have a northwest alignment (Moser, 1977). Multiple levels of cavern development in the area imply that karst development is related to changes in the elevation of base level flow.

BACKGROUND

ACb-3, approximately 70 meters long and 15 meters wide, is developed in exposed Tuscumbia Limestone (Unit A) about 120 feet above present river level. The main room has both an east-west and northwest orientation with side passages aligned to the northeast (Fig. 2). The cave contains vertebrate fossils, significant both in number and type, that are associated with deposits of secondary calcium carbonate (speleothems). A basal silty clay, (Unit B) which extends throughout most of the cave, does not contain any faunal remains. Sediments (Units H, D, E) deposited above this sterile layer are fluvial or colluvial in origin (Bell and Lamb, 1987) and all contain vertebrate remains. Bones include those of sloths (*Megalonyx jeffersoni*), bats, rodents, and the first record of a sabertooth cat (*Smilodon*) in Alabama. A list of the vertebrate fauna is given in Table 1. Within and overlying the sediments are the layers of flowstone that were sampled for U-series dating.

A southwest trending tunnel near the probable Pleistocene entrance (Fig. 2) contains bones from several sloths. At the back of this tunnel, there is a dig that is suspected to be part of a 19th century excavation reported on by Joseph Leidy in 1855, where he described the first *Megalonyx jeffersoni* in Alabama (Bell, 1985).

The cave sediments and bone specimens in ACb-3 were studied and described by G. Bell, Jr., James Lamb, Jr., and Susan Henson, of the Red Mountain Museum. Stratigraphic and lithologic descriptions are most comprehensive at exposures where flowstone occurs, although similarities in some of the strata make accurate identification difficult. Extension of stratigraphic units under flowstone terraces are inferred from available exposures. Speleothems were sampled by Bell and Lamb and dated by Richard Lively at the Minnesota Geological Survey. Seven flowstone samples were collected in 1985 from cross-sectional areas identified on Figure 2 as X-X', Y-Y' and Z-Z'. In 1986, additional samples (6b, 6c, 7b, 7c) were collected along Z-Z', and in 1987, calcite soda-straw fragments (small, hollow stalactites) embedded in the channel fill near X-X'

Table 1.-Fauna identified in cave ACb-3. Refer to Figures 2 and 3 for locations of sedimentary units.

Unit D – Clayey sediment resting upon basal silty clay.
- At cross section Z – Z':
  - Upper Unit – may be equivalent to Unit E in other parts of ACb-3
    - *Megalonyx jeffersoni*
    - *Odocoileus virginianus*
  - Lower Unit
    - *Megalonyx jeffersoni*
    - *Odocoileus virginianus*
    - *Sylvilagus ? sp.*
    - *Sciuridae*
- At cross section Y – Y':
  - *Megalonyx jeffersoni*
  - *Sylvilagus ? sp.*
- Main cave other than noted cross sections:
  - *Dasypus bellus*
  - *Lynx rufus*
  - *Megalonyx jeffersoni*
  - *Mylohyus nasutus*
  - *Tapirus sp.*
  - *Canis sp.*
  - *Felidae.*
  - *Anura*

Unit E – Rimstone pools, side tunnel
- Between X – X' and Y – Y':
  - *Tapirus sp.*
  - *Mylohyus nasutus*
  - *Megalonyx jeffersoni*
    - Adults and infant
  - *Dasypus bellus*
  - 22 other small vertebrates

Unit H – Channel fill on basal silty clay
- At cross section X – X':
  - *Blarina sp.*
  - *Neotoma sp.*
  - *Microtus sp.* (2)
  - *?Spilogale putoris*
  - *Sylvilagus ? sp.*
  - *Sciuridae*
  - *Anura*
  - *Chiroptera (2+?)*
  - *Colubridae*

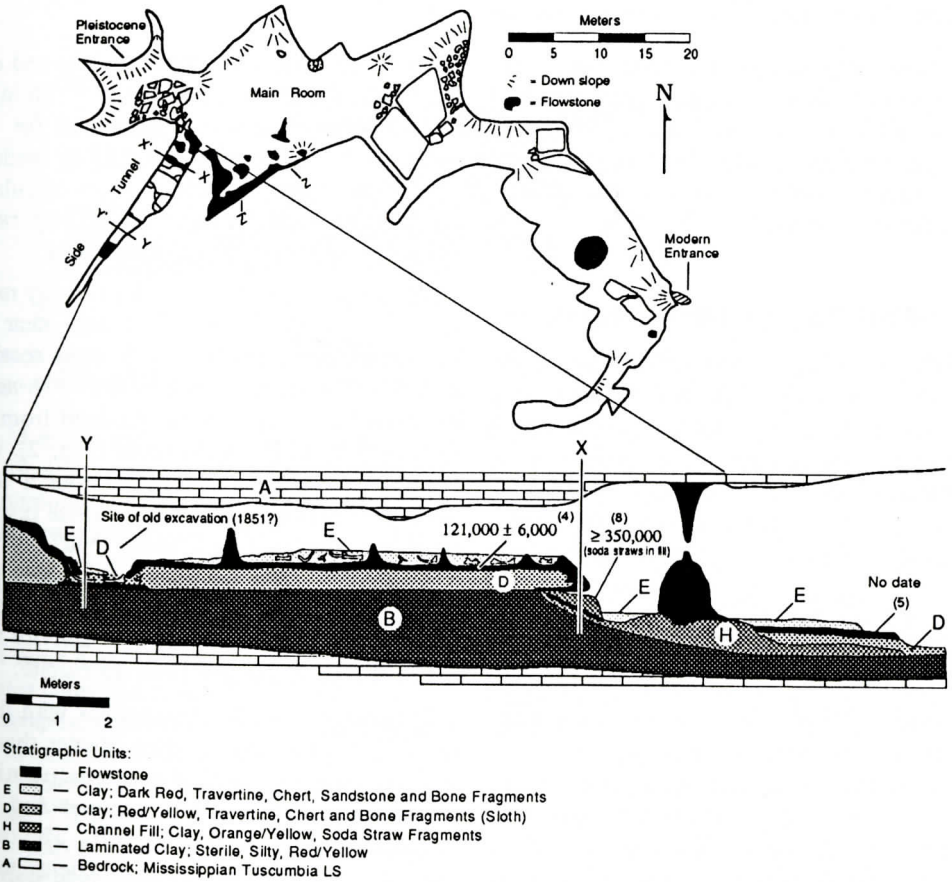

Figure 2.-Plan view of cave ACb-3. Side tunnel, showing locations of flowstone deposits and cross sections relative to the sediments and bone deposits. Numbers in parentheses refer to the sample numbers in Table 2.

Table 2.-Uranium and thorium concentrations, activity ratios and calculated ages.

Sample #	U Conc. (ppm)	Th Conc. (ppm)	$^{234}U/^{238}U$	$^{230}Th/^{234}U$	$^{230}Th/^{232}Th$	Age (x1000 yrs)*	Comment
ACb3-1-1285	2.040±0.040	0.52	1.133±0.013	0.905±0.021	12.4±0.4	228±15	
ACb3-2-1285	0.500±0.010	0.06	0.977±0.018	0.792±0.020	20.8±1.1	172±10	
ACb3-3a-1285	0.377±0.006	0.08	1.222±0.020	0.669±0.015	11.5±0.4	115±4	Top
ACb3-3b-1285	0.465±0.009	0.08	0.995±0.018	0.671±0.017	11.9±0.6	121±6	Bottom
ACb3-4-1285	0.403±0.008	0.06	1.097±0.023	0.680±0.018	15.0±0.8	121±6	Bottom
ACb3-5-1285	0.320±0.006	0.34	1.006±0.013	1.235±0.025	3.6±0.1		
ACb3-6a-1285	0.262±0.005	0.19	1.090±0.022	0.484±0.015	2.2±0.1	<71	Top
ACb3-7a$_1$-1285	0.220±0.004	0.09	1.088±0.023	0.497±0.017	4.0±0.2	<74	Middle
ACb3-7a$_2$-1285	0.214±0.003	0.14	1.061±0.018	0.655±0.018	3.2±0.1	<114	Bottom
ACb3-6b-0786	0.790±0.009	0.58	1.115±0.011	0.470±0.009	2.2±0.1	<68	Top
ACb3-7b-0786	0.238±0.003	0.05	1.032±0.018	0.457±0.011	7.6±0.4	<66	Bottom
ACb3-6c-0786	0.660±0.010	0.68	1.070±0.018	0.745±0.017	2.4±0.1	<145	Top
ACb3-7c-0786	0.262±0.005	0.22	1.033±0.021	0.771±0.018	2.9±0.1	<158	Bottom
ACb3-8-0087	0.415±0.006	0.06	1.555±0.020	1.004±0.022	33±3	≥350	Soda straws

*Calculated ages based on the following values for λ: ^{234}U, 2.794×10^{-6} yr^{-1}; ^{230}Th, 9.21×10^{-6} yr^{-1}; ^{228}Th, 9.92×10^{-4} day^{-1}; ^{224}Ra, 1.904×10^{-1} day^{-1}.

Samples with < ages have $^{230}Th/^{232}Th$ activity ratios less than 10.

were also collected. Several soda-straw fragments were selected from the collection and processed as one sample. One attempt was made to radiocarbon date a bone fragment, but the laboratory could not recover enough collagen for an analysis.

RESULTS AND DISCUSSION

Speleothem ages were determined at the Minnesota Geological Survey laboratory using the U-series dating method (Thompson, 1973) with some modification to the procedures for separating U and Th by ion-exchange. Isotopic activities were measured with an alpha spectrometer. Activity ratios, U concentrations, and $^{230}Th/^{234}U$ ages with one-sigma errors are given in Table 2. U concentrations range from 0.21 to 2.0 ppm and Th concentrations from 0.05 to 0.68 ppm.

The low $^{230}Th/^{232}Th$ activity ratios indicate that detrital thorium may be present in the calcite. A reliable radiogenic age assumes that no ^{230}Th was incorporated at the time the calcite precipitated. If some ^{230}Th was included, as part of a detrital residue for instance, a date calculated from the $^{230}Th/^{234}U$ activity ratio would be older than the date calculated without initial ^{230}Th (Schwarcz, 1980, Milske and others, 1983). Because the activity of ^{230}Th in the detrital phase was not be measured for this study, no correction was assumed or made to the ages reported in Table 2. Ages calculated for samples with $^{230}Th/^{232}Th$ activity ratios below 10 are shown as 'less-than' dates.

All samples with $^{230}Th/^{232}Th$ activity ratios above 10 are from the side tunnel near the Pleistocene entrance (Figs. 2, 3; cross sections at X, Y). The samples with $^{230}Th/^{232}Th$ activity ratios less than 10 were obtained from the shelf at Z-Z' in the main room (Fig. 2). One sample, ACb-5-1285, collected from a layer (Fig. 2) of non-laminar, friable calcite crystals (possibly deposited in a pool), had a $^{230}Th/^{234}U$ activity ratio significantly greater than unity. This may have resulted from detrital ^{230}Th contamination ($^{230}Th/^{232}U$ activity ratio = 3.6) or loss of uranium from the calcite.

Speleothem ages for the samples with detrital $^{230}Th/^{232}Th$ activity ratios greater than 10 are consistent both with the internal stratigraphy of individual flowstone samples and with the sequence of flowstone deposits. The top of flowstone sample #3 is equivalent to or younger than the bottom (Table 2, #'s 3a, b), and dates from the base of the flowstone above

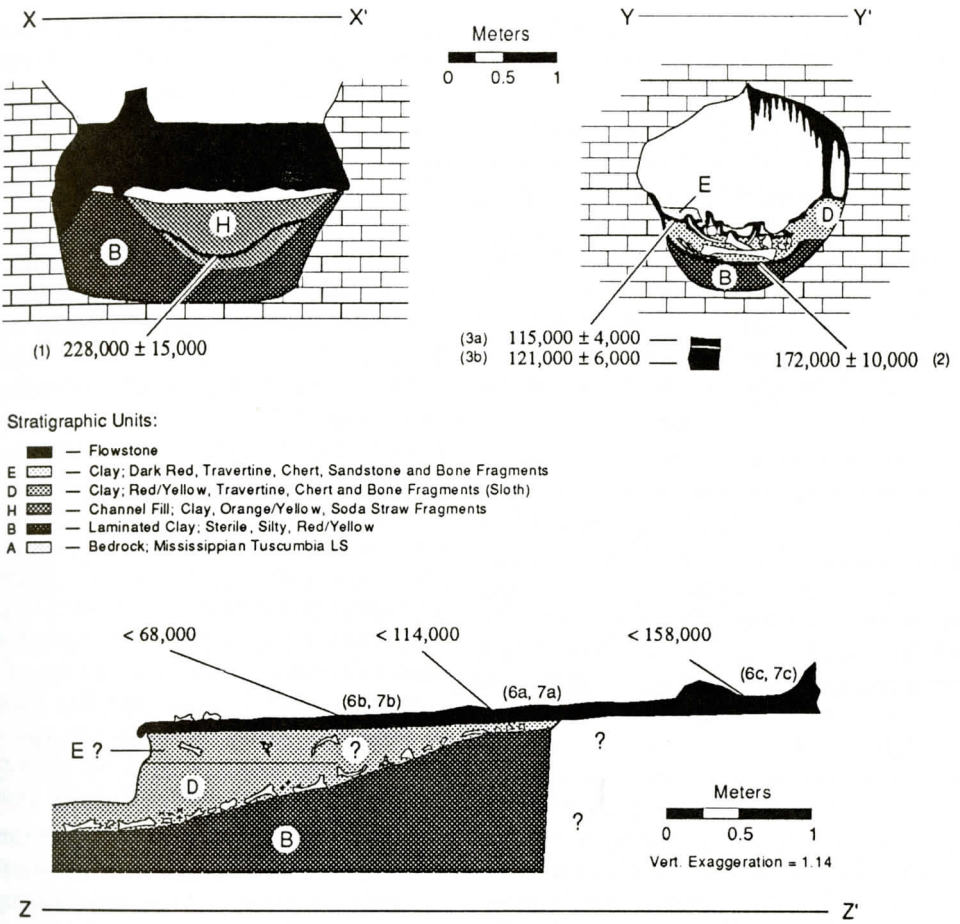

Figure 3.-Cross sections showing U-series dates relative to the stratigraphic sequence of the flowstone, bones and sediments at those locations. Numbers in parentheses refer to the sample numbers in Table 2.

unit D in the side tunnel (Table 2, #'s 3b, 4, Figs. 2, 3) are equivalent. The sequence of oldest to youngest ages is also in accordance with the flowstone/sediment stratigraphy (Table 2, Figs. 2, 3). Sample #'s 2 and 8 (Table 2), with the highest $^{230}Th/^{232}Th$ activity ratios are the least likely to show any detrital ^{230}Th effects. Both have ages consistent with the other carbonates dates and with the sediment-flowstone stratigraphy. Dates from the flowstone shelf at Z-Z' also show a consistent vertical stratigraphy (Table 2) even though their potential for detrital ^{230}Th contamination is greater ($^{230}Th/^{232}Th$ activity ratios <10). The maximum ages reported also decrease systematically in one direction. It is possible that detrital ^{230}Th may not be a significant problem in these samples but, if it is, the ^{230}Th contamination is more likely to be of a systematic rather than random nature.

The passage morphology and sediment record imply that cave ACb-3 first developed as a phreatic system and later evolved into a vadose cave. The basal sedimentary unit (B), is composed of thinly laminated clay and silt, indicative of an influx of fine sediment and deposition in still water. This unit does not contain any bone or secondary calcite. A fluvial channel, filled with sediment, cuts into unit B within the main room (Fig. 2). The channel fill (H) consists of orange to yellow clay that may be partially reworked basal sediment from unit B and contains a large number of soda straw fragments and small animal bones. Channels,

fluvial sediments and secondary carbonates above unit B mark the change to a vadose environment.

The fauna in cave ACb-3 were originally thought to be late Wisconsinan in age because of proximity to a nearby cave, ACb-2, that is at a lower elevation and contains radiocarbon dated bone fragments that are <26,000 RCYBP. U-series dates of speleothem deposition in ACb-3 however, indicated that the ACb-3 bone deposits were substantially older than late Wisconsinan and extended into the Illinoian glacial period.

The oldest secondary carbonates recovered in the cave are the soda-straw fragments from the fluvial channel-fill (H) above unit B (Fig. 2). Assuming that the soda-straws developed on the ceiling, in an air-filled cavity, and only later were incorporated into the channel-fill, their formation imply that the cave evolved from a phreatic to a vadose environment some time prior to the soda-straw equilibrium date of ≥350,000 years B.P. Although the incorporated soda-straws do not date the channel-fill, a flowstone layer within unit H (X-X', Fig. 2, 3), has an age of 228,000 ± 15,000 years B.P. Faunal remains in the channel fill above the flowstone layer (at X-X') include bats, rodents, voles, snakes, squirrels and other animals of similar size.

Larger animals (sloth, deer) gained access to the cave after 172,000 ± 10,000, but before 121,000 ± 6,000 years B.P. This is demonstrated by semi-articulated to relatively complete remains of individual animals in the deposits of unit D, a red to yellow clay mixed with chert, travertine, and bone fragments. The 172,000 year date was obtained from a flowstone layer at the base of unit D sediments and the 121,000 year age from flowstone at the top of unit D (Table 2, sample# 2; Figs. 2, 3; Y-Y'). The presence of large animals in the cave after 172,000 years B.P. indicate that a new, larger entrance had developed, possibly near the west end of the cave (Fig. 2). The position of bones at several of the sloth excavation sites indicates that the animals died after entering the cave. Twelve individual sloths have so far been identified, and the cave appears to have been continually visited by a variety of animals following 172,000 years B.P.

A fourth period of speleothem deposition is represented by the extensive rimstone pools just southwest of cross section X-X' and extending beyond cross section Y-Y' (Figs. 2, 3). Ages of 121,000 ± 6,000 years were obtained for two samples from the base of the flowstone (Table 2; sample# 4, Fig. 2; sample #3b, Fig. 3, Y-Y') and an age of 115,000 ± 4,000 years (Table 2; sample# 3a, Fig. 3, Y-Y') was obtained for the top of the flowstone deposit. The flowstone and rimstone pools were buried by another layer of sediment (unit E; Fig. 2). Sediment in unit E, like the other units, is composed primarily of clay and silt and contains chert and sandstone fragments. This unit contains bones from several large animals including adult and young sloths (*Megalonyx jeffersoni*), as well as 22 species of small vertebrates. Unit E lacks overlying flowstone to provide a younger limit on the age of the sediment, and thus it could have been deposited any time during the past 115,000 years.

A large bone taken from one of the rimstone pools did not have enough measurable collagen to obtain a radiocarbon age, and thus supports the interpretation that the bone beds are older than late Wisconsinan.

On the south side of the main room, just east of cross section X-X' (Fig. 2) an extensive flowstone shelf has accumulated on bone-bearing sediments thought to be equivalent to units D and E (Fig. 3, Z-Z'). Due to the possibility that detrital ^{230}Th may have been included with the calcite when it precipitated, the calculated ages for these samples are reported as maximum ages. The data as shown, indicate that the flowstone shelf at Z-Z' has a maximum age of 158,000 years and appears to become younger to the northeast (in the direction of Z on the cross section, Fig. 3). Further study of this material is warranted because (1) better flowstone dates at Z-Z' could provide a younger time limit on the deposition of unit E sediments, if they can be reliably placed at this location, and (2) the sequence would provide a

date for the last major period of flowstone accumulation and sediment deposition in that part of the cave.

SUMMARY

U-series dating has been used to establish a preliminary chronological sequence of sediment deposition and flowstone formation within ACb-3, a bone-bearing cave in northwestern Alabama. The calculated ages are uncorrected for potential detrital ^{230}Th and are therefore interpreted to represent maximum dates of calcite precipitation.

On the basis of the present data we suggest that the cave began as a small phreatic system, accumulating layers of fine clay and silts without bones or speleothems. Prior to 350,000 years B.P., ACb-3 evolved into a vadose cave and calcite soda-straw stalactites began to form. Some of the soda straws (≥350,000 years B.P.) fell from the ceiling and were incorporated into channel-fill sediments (unit H). These sediments also contain bones of small animals and a layer of flowstone deposited 228,000 ± 15,000 years B.P.

Within the side tunnel heading southwest from the main room, flowstone was deposited on top of unit B, the sterile clays, 172,000 ± 10,000 years B.P. Sediments in unit D, deposited on top of this flowstone, contain the bones of deer and sloths, the first indication that larger mammals were able to enter the cave. The position of bones at some of the sites implies that the animals were alive when they entered the cave. An extensive period of flowstone deposition between 121,000 ± 6,000 and 115,000 ± 4,000 years B.P. resulted in a thick layer of calcite and rimstone pools overlying unit D. Sediments filling the pools (unit E) contain bones from both large and small vertebrates including adult and young sloths (*Megalonyx jeffersoni*).

In the main room along the south wall, east of the side-tunnel mouth, the sediment sequence consists of the basal clay, the bone-bearing unit D, and sediment thought to be equivalent to unit E in the side tunnel. The sediment is capped by flowstone, with maximum ages ranging between 68 to 158,000 years B.P., but these results may have been influenced by the presence of detrital ^{230}Th in the calcite.

Additional research on the U-series isotope geochemistry could clarify the potential for detrital ^{230}Th contamination and further mapping of the sediments would help to correlate material throughout the cave. Other areas of the cave such as the west-end sinkhole and talus pile, have not been extensively investigated and may produce further information about the faunal history of cave ACb-3.

ACKNOWLEDGMENTS

We thank Dr. John Hall and Dr. Doug Jones of the University of Alabama Museum of Natural History whose programs contributed many helpers to excavate the locality in 1985. Susan Henson's expertise in preparing, identifying, and cataloging the fossils has been indispensable.

REFERENCES CITED

Bell, G.L., Jr., 1985 (Abst.), Ground sloths from a cave near Tuscumbia: Journal of the Alabama Academy of Science, v. 56, no. 3, p. 101.

Bell, G.L., Jr. and Lamb, James, P., 1987 (Abst.), Additional investigations in northwest Alabama caves: Journal of the Alabama Academy of Science, v. 58, no. 3., p. 99.

Currin, C., Jr., Copeland, C.W., Jr. and Shannon, S.W., 1976, Summary report of a short-term investigation of late Pleistocene and early Holocene deposits occurring along the Tennessee-Tombigbee waterway in Alabama: Second Supplemental Environmental Report Continuing Environmental Studies Tennessee-Tombigbee Waterway, v. 6, Appendix C, p. 1-102.

Ivanovich, M. and Harmon, R. S., eds., 1982, Uranium series disequilibrium: Application to environmental problems, Clarendon Press, Oxford, 571 p.

Kurten, B. and Anderson, E., 1980, Pleistocene mammals of North America: Columbia University Press, 442 p.

Lively, R. S., 1983, Late Quaternary U-series speleothem growth record from southeastern Minnesota: Geology, v. 11, p. 259-262.

Milske, J. A., Alexander, E. C., Jr., and Lively, R. S., 1983, Clastic sediments in Mystery Cave, Southeastern Minnesota: NSS Bulletin, v. 45, p. 55-75.

Moser, P., 1977 (Abst.), The correlation and signifi-

cance of some solution, structural and weathering features in northwest Alabama: Journal of the Alabama Academy of Science, v. 48, no. 3, p. 75.

Schwarcz, H. P., 1980, Absolute age determination of archaeological sites by uranium series dating of travertines: Archeaometry, v. 22, p. 3-24.

Szabo, M. W., 1975, Geology and mineral resources of the Pride Quadrangle, Alabama: Quadrangle Series Map 4, Geological Survey of Alabama, 18 p.

Thompson, P., 1973, Speleochronology and late Pleistocene climates inferred for O,C,H,U and Th isotopic abundances in speleothems [Ph.D. thesis]: Hamilton, Ontario, McMaster University, 340 p.

Womochel, D. R., 1982 (Abst.), The Winston Cave local fauna and the Late Pleistocene faunal gradient in eastern North America: Journal of the Alabama Academy of Science, v. 53, no. 3, p. 51.

SOUTHEASTERN GEOLOGY
V. 33, No. 1, October 1992, p. 9-21

THE POSTMETAMORPHIC APPLING GRANITE, GEORGIA: ORIGIN OF FACIES AND LARGE MAFIC ENCLAVES IN A COMPOSITE GRANITE

Robert L. Nusbaum[1], James D. Green[1], Nancy Whiting[1]
Debra S. Stakes[2], and Michael D. Glascock[3]

[1]Department of Geology
College of Charleston
Charleston, SC 29424

[2]Department of Geosciences
University of South Carolina
Columbia, SC 29028

[3]Research Reactor Facility
Research Park
Columbia, MO 65211

ABSTRACT

The late-Paleozoic Appling Granite is comprised of two facies; a high-silica, medium-grained facies (MF), and a porphyritic facies (PF). Over half of the pluton consists of the biotite-PF which has abundant alkali feldspar megacrysts (up to 8 cm in length) surrounded by a medium-grained, hypidiomorphic-granular groundmass. The MF consist of quartz, alkali feldspar, plagioclase, biotite, muscovite and accessory Fe-Al-Mn garnet. Micrographic intergrowths of quartz in alkali feldspar are optically continuous and cuneiform in the MF. Field study indicates that the transition from MF to PF is gradational, with a weakly porphyritic zone between the MF and PF. Within this zone, we measured alkali feldspar megacrysts up to 1.0 cm in length.

Large mafic enclaves (LME) are porphyritic with perthitic alkali feldspar megacrysts surrounded by groundmass consisting of minerals which are compositionally and texturally identical to those in PF samples. The primary difference between the PF and the LME is greater abundances of biotite, magnetite, titanite, and allanite within the LME. Cumulate layering was not observed in the LME. Whole-rock oxygen isotope ratios and whole-rock geochemistry indicate that the LME may be comingled trachybasaltic, or high-K basaltic magma which was metamorphosed by the host silicic magma.

The consanguineous nature of the PF and MF is supported by field and geochemical data. Following substantial crystallization of the PF, relatively rapid crystallization of the MF occurred in symphony with vapor exsolution from the melt phase. Micrographic texture in the MF may have resulted from nonequilibrium kinetically driven conditions accompanying the ascent of the magma.

INTRODUCTION

An arcuate chain of texturally similar granitoid plutons of late-Paleozoic age extends from Maryland into Georgia (Sinha and Zietz, 1982). Areal exposures of these plutons cover an estimated 10,000 km^2, making this one of the most prolific magmatic events in the development of the Southern Appalachians (Sinha, 1988). Most of the granitic plutons are composite bodies containing a coarse-grained porphyritic facies which is commonly associated with either a medium-grained facies or a fine-grained facies, or both (Speer and others, 1980; McSween and others, 1991). Compositional facies are also recognized by the presence or absence of minerals such as hornblende, muscovite, cordierite, and garnet (Speer and others,

1980).

Compositional facies changes are gradational in nature, suggesting that they occurred in response to changing magmatic conditions (Speer and others, 1980). Relatively abrupt changes in texture observed in some of the better exposed composite plutons (e.g., Liberty Hill Pluton; Speer, 1987) are interpreted to reflect multiple intrusion events involving genetically related magma. For example, fine-grained biotite granite in the Liberty Hill Pluton is interpreted to have evolved from interstitial melt extracted from magma crystallizing to form coarse-grained rock (Speer, 1987). The extracted melt was probably vapor-rich, facilitating rapid crystallization of the finer-grained granitoid facies (Speer and others, 1989).

The Appling Granite is located in the Kiokee Belt of the southern Appalachian Piedmont in eastern Georgia. Although the absolute age of the Appling Granite has not been determined it has been grouped with other unmetamorphosed late-Paleozoic granitoids on the basis of its texture and mineralogy (Fullagar and Butler, 1979). The purpose of this study is to examine the Appling Granite facies petrographically and compositionally with the goal of understanding the origin of its facies. Large mafic enclaves were also analyzed to examine models for their origin.

FIELD RELATIONS OF THE APPLING GRANITE

The Appling Granite is a composite pluton (Figure 1) consisting of: 1) roughly 16 km^2 of porphyritic facies (PF), biotite granite with conspicuous alkali feldspar megacrysts; and 2) about 12 km^2 of medium-grained facies (MF), biotite-muscovite-garnet granite. Based on available field exposures, the transition from MF to PF appears to be gradational with a weakly porphyritic zone which was observed between the MF and PF. Within this zone, we measured alkali feldspar megacrysts up to 1.0 cm in length.

Scarce biotite-, magnetite-, titanite-, and allanite-rich mafic enclaves occur in the PF. Although volumetrically insignificant, they are unusually large, ranging in size from about 2 m to 5 m in diameter and are designated as large mafic enclaves (LME) to distinguished them from smaller, but more common biotite-schlieren and foliated, country-rock xenoliths. Observed contacts between PF and LME are not sharp. Contacts with smaller mafic enclaves and biotite-schlieren are sharper and may have biotite enrichment along the contact. Grain size in mafic enclaves and schlieren is typically smaller than that in LME. Mafic schlieren and xenoliths were studied petro-

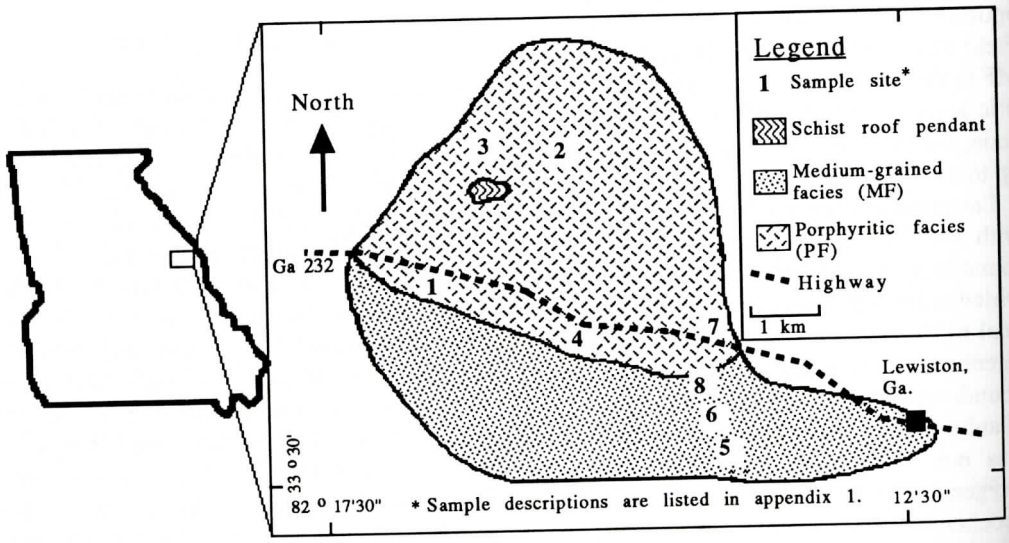

Figure 1. Geologic map of the Appling Granite.

graphically; only the LME were studied in sufficient detail to warrant further discussion.

The Appling Granite is cross-cut by pegmatite and aplite dikes. PF exposures typically display an alignment of alkali feldspar megacrysts in circular to elliptical patterns ranging in diameter from 1-10 m. Systematic orientation of alkali feldspars was not observed.

ANALYTICAL PROCEDURES

Twenty-five samples were selected for study. Many of the PF and LME samples were collected from the only major quarry in the Appling Granite (Sample site 4, Figure 1). Several other exposures were studied; however the flat surfaces of the exposures restricted availability of suitably unaltered rock. MF samples were collected from residual boulders in fields.

Mineral compositions for three representative samples were determined on a Cameca SX-50 electron microprobe equipped with four wavelength-dispersive spectrometers at the Department of Geological Sciences, University of South Carolina. A beam current of 15nA and an acceleration voltage of 15 kV were used in conjunction with a 3 μm beam. Natural mineral standards were provided by the Smithsonian Institution. Data reduction was performed using the PAP technique developed by Cameca which allows on-line formula calculation to check the quality of analyses. Precision errors are 1% or less for concentrations >0.5wt%.

Whole-rock major elements and Rb, Sr, Ba, Pb, Zr, and Zn abundances were measured for 15 samples by X-ray fluorescence spectrometry at X-ray Assay Laboratories, Don Mills, Ontario. Samples were analyzed in duplicate, except for AP 19 and AP 20 which were analyzed in quadruplicate. Rare earth elements (REE) were determined for 7 samples by instrumental neutron activation analysis (INAA) at the Research Reactor Facility, University of Missouri-Columbia (see Graham and others, 1982 for INAA procedure and precision estimates). Due to the large crystal size of some samples, 1 kg samples were crushed and split for XRF and INAA.

Oxygen isotope ratios were analyzed using hand-picked mineral separates for each facies within the Appling Granite. An exception is the matrix feldspar which is mostly plagioclase. Oxygen for the isotopic analyses was liberated by reaction of silicate minerals with ClF_3 in nickel bombs at 550°C as described by Borthwick and Harmon (1982). Oxygen isotope data are reported in standard δ notation relative to the Vienna SMOW standard for oxygen. The standard error of each analysis is approximately ± 0.2 per mil for oxygen.

PETROGRAPHY AND MINERAL CHEMISTRY

Porphyritic Facies

Perthitic alkali feldspar megacrysts account for 30-55 vol% of the PF samples selected for study. Megacrysts (up to 8 cm in length) often contain inclusions of plagioclase, biotite, titanite, and quartz which are oriented parallel to crystal faces. Plagioclase, biotite, and quartz also occur in a 2-5mm, hypidiomorphic-granular groundmass. Normalized to 100 vol%, groundmass minerals have the following abundances: plagioclase (34±8%); quartz (41±7%); alkali feldspar (13±3%); biotite (8±3%); myrmekite (2±2%); titanite (1±1%); and magnetite (1±1%). Allanite is present in most PF groundmass samples studied, exhibiting oscillation zones which are metamict. Accessory minerals include apatite, zircon, chalcopyrite, and pyrite.

Plagioclase displays oscillatory zoning with core compositions typically ranging from An 24-30 and rims, An 24-25 (Table 1A). The most strongly zoned plagioclase analyzed has a difference of 4 mol% An between core and rim. Alkali feldspar megacrysts (Table 1B) are chemically unzoned and perthitic. The analyses represent the unmixed potassic phase only, with the exception of the first analysis of AP17 which was performed while traversing an alkali feldspar megacryst. This analysis best represents an estimate of the original igneous alkali feldspar. The uniform distribution of albite lamellae in perthites suggest that the feldspars

were not compositionally zoned prior to subsolidus reactions.

Biotite occurs in clusters within the groundmass and as inclusions within feldspars, quartz and titanite. Individual crystals of biotite are very weakly zoned as rim compositions are slightly more Fe-rich than cores (Table 1C). Molar Fe/(Fe+Mg) ranges from 0.54-0.56 for cores and 0.53-0.56 for biotite rims (Figure 2).

Medium-Grained Facies:

Grain size typically ranges from 1- 4 mm for the MF. Textures of the MF are micrographic in some samples and allotriomorphic-granular in others. Micrographic intergrowths of quartz (51-52 vol%) in alkali feldspar (37 vol%) are optically continuous and cuneiform. Additional primary minerals include plagioclase (9-10 vol%), biotite (1 vol%), and accessory brownish red garnet and magnetite. Garnet separates were microprobed and are FeO- (21.04 wt%), MnO- (21.41wt%), and Al_2O_3-rich (20.81 wt%). Limited biotite analyses indicate an Fe-enrichment for MF samples compared to PF

Table 1. Representative microprobe analyses.

1A. Plagioclase feldspar

	AP15	AP15	AP15	AP15	AP17	AP17	AP17	AP15
SiO_2	62.93	62.95	63.11	62.45	63.02	63.52	61.34	62.54
Al_2O_3	23.95	23.87	23.74	23.75	24.21	23.77	25.01	23.91
Fe_2O_3	0.05	0.05	0.03	0.03	0.05	0.09	0.04	0.04
CaO	4.91	4.77	4.95	4.64	4.93	4.47	5.80	4.77
Na_2O	7.94	8.03	7.91	8.04	7.96	8.23	7.52	8.09
K_2O	0.18	0.14	0.28	0.15	0.19	0.21	0.20	0.20
Total	99.97	99.80	100.02	99.06	100.36	100.30	99.91	99.56
	Cattions per 8 (O)							
Si	2.776	2.780	2.784	2.779	2.770	2.791	2.718	2.772
Al	1.245	1.243	1.234	1.245	1.254	1.231	1.306	1.249
Fe	0.002	0.002	0.001	0.001	0.002	0.003	0.001	0.001
Ca	0.232	0.226	0.234	0.221	0.232	0.211	0.275	0.227
Na	0.679	0.687	0.676	0.694	0.678	0.701	0.646	0.695
K	0.10	0.008	0.016	0.009	0.011	0.012	0.012	0.11
Total	4.945	4.945	4.945	4.949	4.947	4.948	4.958	4.956
AN	25.2	24.5	25.3	23.9	25.2	22.8	29.5	24.3
Comment	PF core	PF rim	PF core	PF rim	LME core	LME rim	LME inc.	PF inc.

1B. Alkali feldspar

	AP15	AP15	AP17	AP17	AP22
SiO_2	64.10	63.37	64.60	64.33	63.64
Al_2O_3	19.10	19.04	19.10	19.05	18.75
Fe_2O_3	0.00	0.00	0.02	0.04	0.00
CaO	0.00	0.00	0.00	0.00	0.00
Na_2O	1.13	1.23	1.38	0.93	0.74
K_2O	15.20	15.18	15.34	15.87	15.65
Total	99.53	98.82	100.44	100.22	98.78
	Cations per 8 (O)				
Si	2.969	2.960	2.968	2.968	2.975
Al	1.042	1.048	1.034	1.036	1.033
Fe	0.000	0.000	0.001	0.001	0.000
Ca	0.000	0.000	0.000	0.000	0.000
Na	0.102	0.112	0.123	0.083	0.067
K	0.898	0.905	0.899	0.934	0.933
Total	5.010	5.024	5.025	5.022	5.008
AB:OR:AN	10:90:0	11:89:0	12:88:0	8:92:0	7:93:0
Comment	PF	PF	LME	LME	MF gr.

Table 1. Continued.

1C. Biotite						
	AP22	AP22	AP15	AP15	AP17	AP17
SiO_2	34.69	34.60	35.89	36.10	35.53	36.00
TiO_2	2.94	3.09	3.14	3.25	3.72	3.36
Al_2O_3	17.43	17.21	15.91	16.17	15.69	16.20
Cr_2O_3	0.00	0.05	0.0	0.00	0.00	0.00
FeO	22.66	22.97	20.74	19.43	21.62	20.93
MnO	1.24	1.14	0.63	0.65	0.63	0.68
MgO	6.17	6.01	9.39	9.50	9.02	9.18
Na_2O	0.05	0.07	0.06	0.07	0.06	0.08
K_2O	9.86	9.63	10.05	10.06	10.02	9.96
H_2O	3.82	3.81	3.89	3.90	3.90	3.92
Total	98.89	98.60	99.73	99.12	100.19	100.31
	Cations per 24 (O,OH)					
Si	5.444	5.449	5.523	5.549	5.470	5.504
Al	3.225	3.195	2.884	2.929	2.847	2.920
Cr	0.000	0.000	0.000	0.000	0.000	0.000
Ti	0.348	0.366	0.364	0.377	0.431	0.386
Fe	2.974	3.026	2.668	2.498	2.784	2.676
Mn	0.166	0.152	0.083	0.084	0.082	0.088
Mg	1.444	1.410	2.154	2.176	2.069	2.092
Na	0.016	0.020	0.019	0.020	0.019	0.025
K	1.974	1.936	1.973	1.973	1.967	1.942
Fe/(Fe+Mg)	0.68	0.69	0.56	0.54	0.58	0.57
Comment	MF core	MF rim	PF core	PF rim	LME core	LME rim

Crystals were analyzed on several spots; however, data represent one spot only. PF = porphyritic facies; LME = large mafic enclaves; MF = medium-grained facies; inc. = inclusion of plagioclase in alkali feldspar megacryst; gr. = alkali feldspar in graphic intergrowth with quartz. Biotite H_2O calculated assuming 2 formula equivalents.

samples (Figure 2). Muscovite (1-2 vol%) has partially replaced biotite in some samples. Titanite and zircon are common accessories within the weakly porphyritic zone separating the PF and the MF but are scarce or absent in MF samples.

Large Mafic Enclaves

Large mafic enclaves are porphyritic, containing perthitic alkali feldspar megacrysts (17-30 vol%) which are similar in size, composition, and morphology to those in the PF (Table 1B). The alkali feldspar are surrounded by a medium-grained groundmass which is mineralogically identical to PF groundmass. The primary difference between the PF and the LME is greater abundance of biotite (27-35 vol%), titanite (1-3 vol%), magnetite (3-5 vol%) and allanite (up to 1 vol%) in the LME groundmasses (normalized to 100 vol% groundmass minerals). Groundmass quartz is depleted in LME samples (29-35 vol%) compared to PF samples. The volume percent of plagioclase in the groundmass (24-37 vol%) is comparable to values for PF samples.

The most calcic plagioclase (An 32) analyzed occurs as an optically zoned crystal within the groundmass. In general, plagioclase is slightly more calcic in the LME than the PF, although their compositional ranges overlap. LME plagioclase cores are typically An 25-30 with rim compositions of An 22-28. Most crystals analyzed are normally zoned about 2-3 mol% An.

Biotite occurs in clusters associated with titanite and allanite and is essentially unzoned (Fe/[Mg+Fe] = 56-58). A comparison of biotite chemistry among facies (Figure 2) suggests that LME biotite is slightly more Fe-rich than PF biotite; however, this difference is well

within analytical error expected for the microprobe data.

GEOCHEMISTRY

Whole-rock major elements were analyzed to classify the facies within the Appling Granite and provide constraints on possible source areas for the magmas. Trace element compositions were used to constrain the origin of the facies within the Appling Granite and further constrain the possible source area(s). Oxygen isotope ratios for mineral separates were evaluated to estimate the temperature of isotopic equilibration and test for magmatic equilibrium among phases.

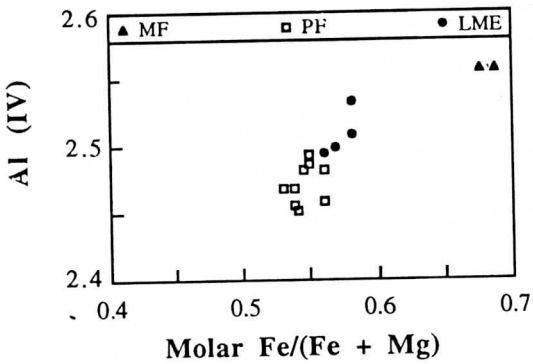

Figure 2. Representative biotite compositions for Appling Granite facies. Values are in structural formula units calculated on the basis of 24 oxygens.

Major Elements

Volatile-free major element compositions of PF and MF are characteristic of metaluminous and peraluminous granite, respectively according to the classification of Shand (1951). The PF is an I-type granite (Chappel and White, 1974) on the basis of its Na_2O abundance, normative corundum composition (Table 2A), and the presence of titanite and brown-green biotite. The MF is transitional between I-type and S-type granite with normative corundum > 1mol%. All facies are calc-alkaline when plotted on an AFM diagram.

Groundmass samples of LME are trachybasalt to high-K basalt according to the classification of Irvine and Baragar (1970).

Trace Elements

Rare earth element (REE) abundances were determined for five PF samples, one MF sample, and one LME sample containing 30 vol% alkali feldspar megacrysts. The REE patterns for the PF exhibit greater variation for light-REE than heavy-REE. Light-REE values exceed chondrite values by 80 to 100 times and La/Lu ratios range from 8-18 (Figure 3A). A negative Eu-anomaly was observed for all PF samples. The magnitude of the Eu-anomaly correlates inversely with increasing La/Lu.

The pattern exhibited by the MF sample is flatter than those for PF samples (Figures 3A and 3B). Light-REE abundances are about 50 times chondritic values with a La/Lu of 3. The magnitude of the negative Eu-anomaly is similar to that for several PF samples.

Interpretation of REE for the LME sample is more difficult because it contains alkali feldspar which may be xenocrystic. The slope of the pattern (La/Lu = 11) is comparable to that of the PF samples. Light-REE chondritic values for LME exceed those of PF samples by nearly three orders of magnitude and heavy-REE by approximately two. These unusually high abundances are attributed to greater modal allanite and titanite in the LME.

Plots of trace element data vs SiO_2 yield mostly scattered trends with the exception of those involving Ba and Sr. The Ba content varies linearly with SiO_2 for PF and MF samples (Figure 4A). The range of Ba values may correlate with the volume of alkali feldspar megacrysts in PF samples (K_D = 6.1; Philpotts and Schnetzler, 1970). The Ba content in the biotite-rich LME is remarkably low considering the apparent compatibility of Ba in the biotite structure of acidic magmas (K_D = 9.7; Higuchi and Nagasawa, 1969).

The variation of Sr with SiO_2 exhibits a steep negative slope (Figure 4B), again suggesting that alkali feldspar abundance may explain the range of Sr variation (alkali feld-

Table 2 A: Representative whole-rock compositions. B: Representative whole-rock trace element abundances.

A	AP24	AP22	AP7	AP14	AP19	AP20
SiO_2	74.76	74.49	70.44	70.54	50.12	48.10
TiO_2	0.15	0.08	0.45	0.49	3.02	3.16
Al_2O_3	14.11	14.10	14.69	14.45	14.57	14.13
Fe_2O_3	1.06	0.89	2.58	2.96	17.01	19.22
MnO	0.09	0.06	0.06	0.06	0.32	0.35
MgO	0.29	0.15	0.71	0.76	3.46	3.58
CaO	0.91	0.98	2.10	2.34	4.07	4.10
Na_2O	3.52	3.68	3.73	3.74	2.78	2.54
K_2O	5.09	5.52	5.08	4.49	3.91	4.01
P_2O_5	0.03	0.02	0.15	0.17	0.73	0.81
Total	99.25	99.77	99.38	99.66	98.16	98.34
LOI	0.85	0.82	0.39	0.31	0.85	0.66
Comment	MF	MF	PF	PF	LME	LME
C.I.P.W. Norms						
ap	0.07	0.07	0.33	0.38	1.71	1.91
il	0.29	0.21	0.87	0.95	6.11	6.45
mt	0.75	0.52	1.85	2.13	12.86	14.66
or	29.85	29.50	30.27	26.76	24.56	25.40
ab	29.55	32.91	31.86	31.98	25.01	23.05
an	4.27	4.83	8.39	9.47	16.40	16.14
di	0	0	0.97	0.95	0	0
hy	0.72	0.40	1.37	1.53	8.97	9.81
c	2.46	1.22	0	0	0.30	0.30
q	32.06	30.35	24.09	25.85	4.07	2.37

B	Whole-rock trace elements (ppm)						
	AP24	AP6	AP14	AP9	AP11	AP16	AP17
Rb	292	182	173	206	164	149	265
Sr	83	356	351	398	340	309	247
Ba	303	1090	813	1270	797	557	763
Pb	43	29	27	27	22	20	17
Zr	69	213	278	236	260	297	950
Zn	42	50	58	52	52	65	196
La	19.71	30.81	63.84	60.16	57.67	64.99	249.35
Ce	39.4	116.4	129.5	124.3	119.0	131.6	507.9
Nd	15.47	36.83	64.35	53.22	58.02	57.22	232.87
Sm	5.15	5.60	8.37	8.13	7.63	8.25	37.96
Eu	0.74	0.95	1.24	1.33	1.19	1.19	4.74
Tb	0.76	0.75	0.84	0.84	0.81	0.81	4.77
Yb	3.72	2.48	2.75	2.66	2.50	2.69	13.34
Lu	0.58	0.35	0.35	0.33	0.32	0.34	1.73
Comment	MF	PF	PF	PF	PF	PF	LME

Total equals the sum of oxides plus LOI (loss on ignition). Calculation of Fe+2/Fe(total) assumes ratio of 0.60 corresponding to average granite of Le Maître (1965). Major element composition and Rb, Sr, Ba, Pb, Zr, and Zn for LME were determined on samples which were separated from alkali feldspar megacrysts. REE analyses for LME includs alkali feldspar megacrysts. Rb, Sr, Ba, Pb, Zr, and Zn anlayzed by X-ray fluorescence. REE analyzed by instrumental neutron activation.

spar K_D = 3.9; Philpotts and Schnetzler, 1970). Lower Sr in MF may reflect greater quartz and lower modal plagioclase and alkali feldspar in the MF.

Oxygen Isotope Ratios

Variation in $\delta^{18}O$ values among minerals from the same rock can be used to determine the history of isotopic exchange for the system. For example, the equilibrium values of Δ_{QAF} ($\delta^{18}O^{quartz}$ - $\delta^{18}O^{alkali\ feldspar}$) are different than those expected for Δ_{QB} ($\delta^{18}O^{quartz}$ - $\delta^{18}O^{biotite}$), or Δ_{AFB} ($\delta^{18}O^{alkali\ feldspar}$ - $\delta^{18}O^{biotite}$). Such variation is attributed to different closure temperatures accompanying isotopic exchanges among the minerals.

Fluids circulating through granitic rocks will react with feldspars much more readily than quartz (Criss and Taylor, 1986). As a result, Δ_{QAF} is an indicator of magmatic equilibrium in granites when values occur in the range of +1.0 to +1.5 (Taylor, 1968, 1978; Ayuso and others, 1988). For this reason, a comparison of Δ_{QAF} values among minerals in the Appling Granite facies and LME (Table 3) suggests that magmatic, isotopic partitioning exists for the MF and LME samples (Figure 5). The Δ_{QAF} for the PF is slightly depleted compared to the two other samples. This could have resulted from exchange of the PF feldspar with an exsolved fluid phase, or meteoric water. Slower cooling rocks (e.g., PF) probably experienced a longer-lived exchange history with local hydrous fluids. Exchange of local hydrous fluids with the PF may have been limited; however, as alkali feldspar $\delta^{18}O$ is within the range of values for unaltered I-type granite (7-8 °/oo; Taylor, 1968, 1978).

Temperatures established during isotopic equilibration were estimated for the MF, PF, and LME (Table 3). These correlate with Δ_{QAF} because the highest temperature facies (MF = 750°C) also has the lowest Δ_{QAF}. The LME temperature estimate is 700°C and the PF, 400°C. Although these estimates are unconfirmed by additional geothermometry, they are internally consistent with observed isotopic partitioning (e.g., Δ_{QAF}) among minerals within the rocks.

DISCUSSION

Features that distinguish the Appling Granite among other late-Paleozoic granitoids are: 1) LME which have similar mineralogy to the host PF; 2) the presence of micrographic tex-

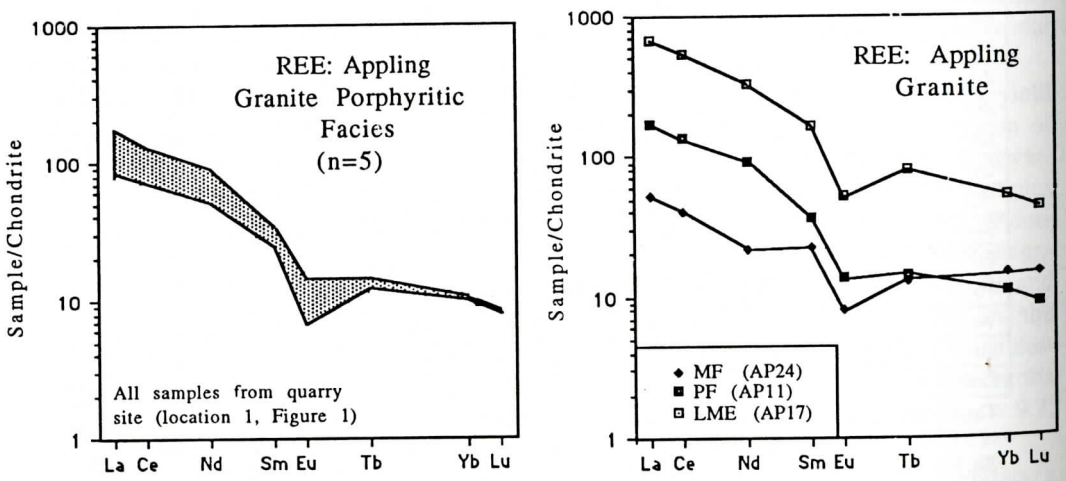

Figure 3 A. Range of compositions for C-1 chondrite-normalized (Taylor, 1980) rare earth (REE) abundances of five Appling Granite PF samples. B. C-1 chondrite-normalized (Taylor, 1980) abundances of rare earth elements for three Appling Granite samples.

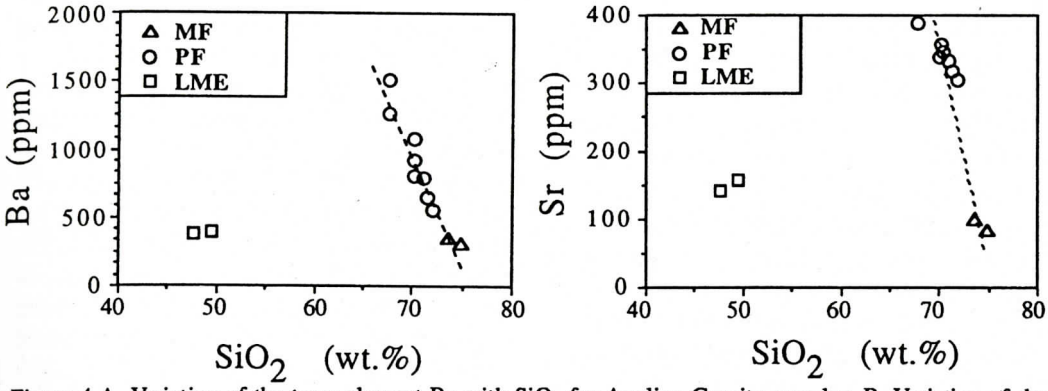

Figure 4 A. Variation of the trace element Ba with SiO_2 for Appling Granite samples. B. Variation of the trace element Sr with SiO_2 for Appling Granite samples.

Table 3. Oxygen isotopes.

Mineral	δO18 (‰)	δO18 (‰)	δO18 (‰)
	PF	MF	LME
Alkali feldspar	7.1	8.0	8.3
Matrix feldspar*	7.9	8.0	8.4
Muscovite		5.6	
Biotite	3.7	5.2	4.6
Titanite	5.1		4.0
Quartz	8.7	8.9	9.3
Δ_{QAF}	1.6	0.9	1.0
T(°C)	400	750	700
* mostly plagioclase			

ture in the MF; and 3) a transitional zone which is slightly porphyritic between the coarser-grained PF and the MF. These features will be used to explain the origin of the LME and MF with respect to the PF of the composite pluton.

Large Mafic Enclaves

The origin of mafic enclaves in most late-Paleozoic granitoids in the Southern Appalachians has been enigmatic because of their characteristically small size, scarcity, and limited study. Speer and others (1989) attributed the schlieren in the Liberty Hill Pluton to disaggregation of mafic material which originated by the one of the processes: assimilation of xenoliths, magma mingling and mixing, or restite unmixing. Others have interpreted the mafic enclaves as autoliths or skialiths (Speer and others, 1980). Mineral compositions and

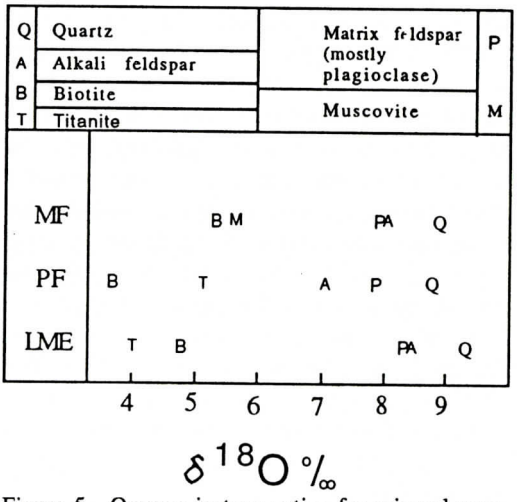

Figure 5. Oxygen isotope ratios for mineral separates within the LME (AP17), PF (AP8), and MF (AP22). Mineral separates were pure with the exception of the matrix feldspar which is mostly plagioclase.

modal abundances of hydrous phases led Whiting and Nusbaum (1989) to suggest that the mafic enclaves in the Appling Granite are disrupted segregations resulting from magma inhomogeneity with respect to water.

Three possible models for origin of Appling Granite LME are considered: 1) xenoliths of disrupted country rock incorporated during intrusion; 2) magmatic mafic segregations, or autoliths; and 3) co-mingled mafic magma. The Appling Granite intrudes Precambrian migmatitic biotite-amphibole paragneiss, leucocratic paragneiss, and sillimanite schists which are intruded by sheets and plugs of orthogneiss and granite (Secor, 1987). Our field study indicates that all of the aforementioned country rocks are present near the margins of the Appling Granite. Xenoliths of these rocks are readily distinguished from LME on the basis of foliation and sharp contacts with PF. Thus, it is unlikely that the LME are partially assimilated country rock xenoliths.

The choice between the autolith model (model 2) and co-mingled mafic magma (model 3) is complex. Both models require that LME were carried upward in the granite from depth; however, they differ as to the nature of the materials from which the LME were derived. Studies of the Lilesville Granite and Pee Dee Gabbro (Speer and others, 1980), and several granitoids of the Sierra Nevada Batholith (e.g., Barbarin, 1991) indicate that co-mingled mafic enclaves typically occur as pillows which are finer-grained than granitic hosts. Generally, smaller mafic enclaves are finer-grained due to quenching. Slower cooling in larger enclaves results in increased grain size toward the center of the enclave and greater chemical reaction between the mafic enclaves and the host granitoid (Barbarin, 1991). The LME in the Appling Granite are not pillow-shaped or fine-grained. They may have, however, experienced extensive chemical reaction with the host PF.

Biotite in the LME is compositionally identical to PF biotite (Figure 2). Study of mafic inclusions in volcanic rocks by Christiansen and Venchiarutti (1990) indicate that selective changes in the composition of mafic inclusions in granitic plutons are expected, particularly with respect to alkalis in the mafic inclusions. These exchanges of components may explain the preponderance of mafic inclusions in Sierra Nevada Mountains which contain hydrous silicates such as biotite and amphibole which are compositionally similar to those in the host granite (e.g., Vernon, 1984; Reid and Hamilton, 1987; Dodge and Kistler, 1988). Feldspar compositional identity has been noted for some Sierra Nevada Batholith mafic enclave-granitoid host pairs (Barbarin, 1991). Appling Granite feldspars are texturally and compositionally nearly identical with the exception of rare calcium-rich cores in a few LME plagioclase cores. Overall, feldspar data are suggestive of equilibration of LME with the PF.

Such identity of mineral compositions has often been cited as support for the autolith model, particularly when isotopic signatures are the same (i.e., Barbarin and others, 1989; Dodge and Kistler, 1990). This is not the case for the PF and LME which exhibit distinctly different oxygen isotopic signatures among mineral separates. The $\delta^{18}O$ values for quartz, feldspars, and biotite in the LME exceed those values in the PF (Figure 5). The LME $\delta^{18}O$ values for quartz, alkali feldspar, and plagioclase also exceed those of MF minerals; whereas MF quartz values are intermediate between PF and LME. These are not trends expected for an isotopically homogeneous, but fractionating magma assuming that quartz $\delta^{18}O$ values are magmatic.

Further isotopic analysis of additional LME within the Appling Granite are required to convincingly distinguish between models 2 and 3. The isotopic heterogeneity exhibited by LME and PF samples favors model 3. Equilibration of mafic magma with cooler chemically distinct silicic magma may result in modification of the mafic components as anhydrous minerals become metamorphosed to hydrous phases during cooling of the granitic magma (Christiansen and Venchiarutti, 1990). Disaggregation and redistribution of the metamorphosed mafic enclaves within the Appling Granitic

magma may have followed such a process.

Appling Granite Facies

The genetic association of finer-grained granitoids and coarse-grained granitoids has been demonstrated (e.g., Speer and others, 1989). Consider the Liberty Hill Pluton, which is the best studied of the Late-Paleozoic granitoids. The fine-grained facies has higher silica, incompatible element enrichment, and compatible element depletion compared to the coarse-grained porphyritic facies; these features are consistent with fractional crystallization (Speer and others, 1989). The texture of finer-grained rock has been attributed to rapid crystallization in the presence of greater vapor accompanying pressure release during emplacement (Speer and others, 1989; Whitney, 1988).

The slightly porphyritic sample between the PF and MF is indicative of a transition zone between the PF and MF. Field relations among the PF, transition zone, and MF suggest that the Appling Granite magma may have crystallized with the PF representing a deeper part of the magma. Support for this is demonstrated by linear plots of Ba vs SiO_2 (Figure 4A) and Sr vs SiO_2 (Figure 4B). Tilting of the pluton southward, followed by erosion could account for the observed field relationships.

The MF of the Appling Granite has the only occurrence of micrographic texture yet reported for postmetamorphic granites in the Southern Appalachians. Although often attributed to eutectic crystallization, graphic texture may also reflect kinetically driven, nonequilibrium conditions (Fenn, 1986). Several possibilities exist including: volatile release accompanying distant surface volcanism; or volatile release accompanying emplacement and crystallization. The former has been used to explain the observed changes in texture within epizonal silicic plutons in the St. Francois Mountains, Missouri (Sides and others, 1981; Nusbaum, 1980). Although this model is intriguing, it is unlikely given the greater depth of emplacement for the plutons in the Kiokee Belt (Vyhnal and McSween, 1990). Alternatively, volatile enrichment within the melt phase accompanying advanced crystallization and melt degassing may be used to explain the observed textural relationships between the MF and PF.

CONCLUSIONS

1. The late-Paleozoic, I-type Appling Granite is a composite pluton comprised of two facies: a 12 km^2 high-silica, medium-grained facies (MF) characterized by micrographic and allotriomorphic-granular texture; and a 16 km^2 porphyritic facies (PF) containing alkali feldspar megacrysts. The contact between MF and PF is gradational with a weakly porphyritic, transition zone which was observed between the MF and PF. Large mafic enclaves (LME) in the PF are biotite, titanite, magnetite, and allanite rich.

2. Mineral compositions for biotite, plagioclase, and alkali feldspar in PF and LME are nearly identical suggesting that LME may be recrystallized, disrupted mafic magmatic segregations which originated at a deeper level within the magma. Oxygen isotopic data for mineral separates contradict an autolithic origin for the LME, however, indicating that they may have originated as co-mingled trachybasalt or high-K basalt magma. If this is true, the compositional identity among minerals may have resulted from metamorphism of the original anyhdrous mafic inclusions.

3. Following substantial crystallization of the PF, relatively rapid crystallization of the MF occurred in symphony with vapor exsolution from the melt phase. Micrographic texture in the MF may have resulted from nonequilibrium kinetically driven conditions accompanying the ascent of the magma.

ACKNOWLEDGEMENTS

Critical reviews by H.Y. McSween, Jr., and J.A. Speer improved the original manuscript. Financial support for field study awarded to J.D. Green by the Southeastern Section Geological Society of America. Microprobe analyses were funded by the Southeastern Regional

Education Board. INAA was made possible by a Department of Energy Reactor Sharing Grant to the University of Missouri Research Reactor.

REFERENCES

Ayuoso, R.A., Horan, M.F., and Criss, R.E.,1988, Pb and O isotopic geochemistry of granitic plutons in northern Maine: American Journal of Science, v. 288A, p. 421-460.

Barbarin, B., Enclaves of the Mesozoic calc-alkaline granitoids of the Sierra Nevada Batholith, California, *in*, J. Didier and B. Barbarin, Enclaves and granite petrology: Elsevier, New York, p. 135-153.

Barbarin, B., Dodge, F.C.W., Kistler, R.W., and Bateman, P.C., 1989, Mafic inclusions and associated aggregates and dikes in granitoid rocks, central Sierra Nevada batholith: Analytic data, U.S. Geological Survey Bulletin, 1899, p. 1-28.

Borthwick, J., and Harmon, R.S., 1982, A note regarding ClF_3 as an alternative to BrF_5 for oxygen isotope analysis: Geochimica et Cosmochimica Acta, v. 46, p. 1665-1668.

Chappel, B.W., and White, A.J.R., 1974, Two contrasting granite types: Pacific Geology, v. 8, p. 173-174.

Christiansen, E.H., and Venchiarutti, D.A., 1990, Magmatic inclusions in rhyolites of the Spor Mountain Formation, western Utah: Limitation on compositional inferences from inclusions in granitic rocks: Journal of Geophysical Research, v. 95, no. B11, p. 17717-17728.

Criss, R.E., and Taylor, H.P., Jr., 1986, Meteoric-hydrothermal systems, *in* J.W. Valley, H.P. Taylor, and J.R.O'Neil, Reviews in Mineralogy, Stable isotopes in high temperature geological processes: Mineralogical Society of America, v. 16, p. 373-424.

Dodge, F.C.W., and Kistler, R.W., 1988, Origin of mafic inclusions, central Sierra Nevada: EOS Transactions of the American Geophysical Union, v. 69, p. 1496.

Dodge, F.C.W., and Kistler, R.W., 1990, Some additional observations on inclusions in the granitic rocks of the Sierra Nevada: Journal of Geophysical Research, v. 95, p. 17841-17848.

Fenn, P.M., 1986, On the origin of graphic granite: American Mineralogist, v. 71, p. 325-330.

Fullagar, P.D., and Butler, J.R., 1979, 325 to 265 m.y.-old granitic plutons in the Piedmont of the Southeastern Appalachians: American Journal of Science, v. 279, p. 161-185.

Graham, C.C., Glascock, M.D., Carni, J.J., Vogt, J.R., and Spalding, T.G., 1982, Determination of elements in National Bureau of Standards' geological standard reference materials by neutron activation analysis: Analytical Chemistry, v. 54, p. 1623-1627.

Higuchi, H., and Nagasawa, H. 1969, Partition of trace elements between rock-forming minerals and the host volcanic rocks: Earth and Planetary Science Letters, v. 7, p. 281-287.

Irvine, T.N., and Baragar, W.R.A., 1971, A guide to the chemical classification of the common volcanic rocks: Canadian Journal of Earth Science, v. 8, p. 523-548.

Le Maître, R.W., 1976, The chemical variability of some common igneous rock: Journal of Petrology, v. 17, p. 589-637.

Le Maître, R.W., Bateman, P., Dudek, A., Keller, J., Lameyre, J., Le Bas, M.J., Sabine, P.A., Schmid, R., Sørensen, H., Streckeisen, A., Woodley, A.R., and Zanettin, B. 1989, A Classification of Igneous Rocks and Glossary of Terms, Blackwell, Oxford.

McSween, H.Y., Jr., Speer, J.A., and Fullagar, P.D., 1991, Plutonic rocks of the Carolinas, *in*, J.W. Horton, Jr., and V.A. Zullo, Geology of the Carolinas: Carolina Geological Society 50th Anniversary Volume, University of Tennessee Press, Knoxville, Tennessee, p. 109-126.

Nusbaum, R.L., 1980, A Precambrian collapse caldera boundary in the St. Francois Mountains, Southeast Missouri, (M.S. thesis): University of Kansas, Lawrence, 77p.

Philpotts, J.A., and Schnetzler, C.C., 1970, Phenocryst-matrix partition coefficients for K, Rb, Sr and Ba, with applications to anorthosite and basalt genesis: Geochimica et Cosmochimica Acta, v. 36, p. 1131-1166.

Reid, J.B., and Hamilton, M.A., 1987, Origin of Sierra Nevada granite: evidence from small scale composite dikes: Contributions to Mineralogy and Petrology, v, 96, p. 441-454.

Secor, D.T., 1987, Regional overview, *in* Secor, D.T., Anatomy of the Alleghanian orogeny as seen from the Piedmont of South Carolina and Georgia: Carolina Geological Society 50th Anniversary meeting 1987 Field Guide, South Carolina Geological Survey, Columbia, South Carolina, p. 1-18.

Sides, J.R., Bickford, M.E., Shuster, R.D., and Nusbaum, R.L., 1981: Calderas in the Precambrian terrane of the St. Francois Mountains, Southeastern Missouri: Journal of Geophysical Research, v. 86, no. B11, p. 10349-10364.

Sinha, A.K., 1988, Plutonism in the U.S. Appalachians: American Journal of Science, v. 288-A, p. ix-xii.

Sinha, A.K., and Zietz, I., 1982, Geophysical and geochemical evidence for a Hercynian magmatic arc, Maryland to Georgia: Geology, v. 10, p. 593-596.

Speer, J.A., 1987, Evolution of magmatic AFM mineral assemblages in granitoid rocks: the hornblende + melt = biotite reaction in the Liberty Hill Pluton, South Carolina: American Mineralogist, v. 72, p. 863-878.

Speer, J.A., Becker, S.W., and Farrar, S.S., 1980, Field relations and petrology of the postmetamorphic, coarse-grained granitoids and associated rocks of the southern Appalachian Piedmont, *in*, D.R. Wones, Proceeding Caledonides in the U.S.A., I.G.C.P. Project 27: Caledonides Orogen: Virginia Polytechnic Institute

and State University, Blacksburg, Virginia, p. 137-148.

Speer, J.A., Naeem, A., and Almohandis, A.A., 1989, Small-scale variations and subtle zoning in granitoid plutons: The Liberty Hill pluton, South Carolina, U.S.A.: Chemical Geology, v. 75, p. 153-181.

Taylor, H.P., Jr., 1968, The oxygen isotope geochemistry of igneous rocks: Contributions to Mineralogy and Petrology, v. 19, p. 1-71.

Taylor, H.P., Jr., 1978, Oxygen and hydrogen isotope studies of plutonic granitic rocks. Earth and Planetary Science Letters, v. 38, p. 177-210.

Taylor, S.R. 1980, Refractory and moderately volatile element abundances in the earth, moon and meteorites: Proceedings of the Lunar and Planetary Science Conference, v. 11, p. 333-348.

Vernon, R.H., 1984, Microgranitoid enclaves in granites--Globules of hybrid magma quenched in a plutonic environment: Nature, v. 309, p. 438-439.

Vyhnal, C.R., and McSween, H.Y., Jr., 1990, Constraints on Alleghanian vertical crustal displacements in the southern Appalachians, based on aluminum-hornblende barometry: Geology, v. 18, p. 938-941.

Walker, G.P.L. , 1989, Gravitational (density) controls on volcanism, magma chambers and intrusions: Australian Journal of Earth Sciences, v. 36, p. 149-165.

Whiting, N.M., and Nusbaum, R.L., 1989, Complex crystallization history of the late-Paleozoic, porphyritic Appling Granite and its mafic enclaves, southern Appalachian Piedmont: Geological Society of America, Abstracts with Programs, v. 21, p. A161.

Whitney, J.A., 1988, The origin of granite: the role and source of water in the evolution of granitic magmas: Geological Society of America Bulletin, v. 100, p. 1886-1897.

APPENDIX: SAMPLE DESCRIPTIONS

Site 1: AP1; schlieren in porphyritic facies.

Site 2: AP2; porphyritic facies from Heggies Rock.

Site 3: AP3, AP4, AP5; biotite-rich, anhedral, microgranular mafic enclaves in porphyritic facies.

Site 4: AP6, AP7, AP8, AP9, AP10, AP11, AP12, AP13, AP14, AP15, AP16; porphyritic facies from quarry. AP17, AP18, AP19, AP20; samples from five meter diameter, medium-grained, biotite-titanite-allanite mafic enclaves (LME) from quarry. AP21; eight centimeter diameter, fine to medium-grained biotite-titanite-allanite mafic enclave.

Site 5: AP22; medium-grained facies with micrographic texture; sample has accessory garnet.

Site 6: AP23; medium-grained facies.

Site 7: AP24; gneissic xenolth in porphyritic facies.

Site 8: AP25; slightly porphyritic granite believed to be transitional between porphyritic facies and medium-grained facies.

SOUTHEASTERN GEOLOGY
V. 33, No. 1, October 1992, p. 23-35

BARRED SHORELINE DEPOSIT IN THE DEVONIAN ELIZABETH SANDSTONE OF WEST VIRGINIA: IMPLICATIONS FOR RESERVOIR BEHAVIOR

ROBIN JOHN MCDOWELL
Department of Geology and Geography
West Virginia University
Morgantown, WV 26506

ABSTRACT

An excellent example of a wave- and tide-dominant shoreline sandstone of the Upper Devonian Catskill delta complex is exposed in outcrops of the Cannon Hill Formation of the Hampshire Group (Famennian) approximately 4 mi (6.4 km) east of Elkins, West Virginia. The outcrops reveal a massive, 54 ft (18 m) thick sandstone, informally named the Elizabeth sandstone. On the basis of: 1) stratigraphic position above marine shales and sandstones and below lagoonal and fluvial sandstones; 2) a vertical sequence of sedimentary structures indicating deposition in shoaling water; and 3) a sequence of sedimentary structures very similar to those found on certain modern, barred, high-energy shorelines, the Elizabeth sandstone is interpreted to represent a regressive foreshore to shoreface sandstone that was deposited in high-energy environments. The excellent exposures near Elkins allow detailed interpretation of shoreface sub-environments such as rip channel, longshore trough, swash bar, and swash face. Documentation of these sub-environments in other ancient sandstones is scarce.

Shoreline sandstones of the Catskill delta complex are significant hydrocarbon reservoirs; however, because exposures of those units are rare, few detailed descriptions exist of outcrop-scale features that may affect reservoir characteristics in Catskill delta shoreline sandstones. Outcrop features of the Elizabeth sandstone near Elkins indicate deposition under conditions of strong wave energy, and numeric models of the Catskill sea indicate that it was mesotidal to low macrotidal; therefore, tidal inlets were probably wide, shallow, and widely spaced. Permeability trends for reservoir sandstones deposited under these conditions would be parallel to depositional strike and uncomplicated by transverse shale breaks or tidal channel lag deposits.

INTRODUCTION

Sandstones of the Upper Devonian Catskill delta complex are important hydrocarbon reservoirs in the central Appalachian basin. (Dennison, 1971). Abundant subsurface stratigraphic data from oil and gas wells in Virginia, West Virginia, and Pennsylvania have provided detailed information on the geometry of Catskill delta reservoir sandstones. Catskill delta shorelines can be placed into three categories on the basis of their shape: digitate, embayed, and straight (Boswell, 1988). The shape of a shoreline is a function of the relative importance of fluvial influx, and wave and tidal reworking (Fisher and McGowen, 1969; Coleman, 1976; Coleman and Prior, 1982). For example, straight shorelines indicate wave domination and have been interpreted to represent deposition in beach and barrier environments (Coleman, 1976; Galloway, 1986). Deltaic sandstones are abundant in outcrops of the Catskill Delta complex; however, because they are parallel to depositional strike wave-dominated shoreline sandstones are well represented only in the subsurface west of the Upper Devonian outcrop belt. Consequently, interpretations of depositional processes for subsurface sandstones rely almost entirely on mapped sand distribution patterns and lack sedimentologic detail. Outcrop-scale features such as internal stratification, frequency and position of shale breaks, permeability distributions, and

directional permeability all significantly affect reservoir characteristics and the movement of fluid across facies boundaries (Tyler and Ambrose, 1986). The potential economic importance of beach and barrier deposits in the Catskill delta complex and other hydrocarbon-producing areas, e.g. the Cretaceous interior of the western U.S. (McCubbin and Brady, 1969; McCubbin, 1982) and the Gulf Coast (Fisher and McGowen, 1969) demands that, where possible, detailed outcrop studies be integrated with subsurface data to increase the understanding of subtle reservoir characteristics and maximize hydrocarbon recovery.

Along US Route 33 approximately 4 mi (6.4 km) east of Elkins, West Virginia, roadcut exposures 1.0 mi (0.6 km) east of the crest of Kelley Mountain (Figs. 1 and 2) reveal what is probably the finest example of a sandy nearshore deposit in the Upper Devonian of the eastern United States. This unit, which correlates with the Elizabeth sandstone of well drillers in the subsurface to the west, has many of the features seen in modern high-energy shorelines. The excellent exposure allows a detailed facies reconstruction which can be used to evaluate the elements that affect reservoir behavior.

Outcrops of the quality discussed here are rare in West Virginia and are usually confined to roadcuts. Furthermore, outcrops represent only small parts of stratigraphic intervals and deposystems. These factors necessarily limit the universality of outcrop-based interpretations. However, the processes that affected deposition of the Elizabeth sandstone, i.e. waves and tides, were probably in operation all along the Catskill Delta shoreline. This may provide insight to other wave- and tide-dominated shoreline sandstones of the Catskill delta complex.

The purpose of this paper is twofold: 1) to describe a unique exposure of an Upper Devonian high-energy shoreline in terms of modern depositional processes; and 2) discuss how internal depositional structures of the Elizabeth sandstone may relate to the movement of fluid in subsurface hydrocarbon reservoirs of similar origin within the Catskill delta complex and other hydrocarbon-producing areas.

STRATIGRAPHIC SETTING

The Upper Devonian Catskill delta complex is part of an extensive, eastward thickening clastic wedge that prograded westward into the Appalachian foreland basin in response to the Acadian orogeny (Ettensohn, 1985). In the vicinity of Elkins, West Virginia, the Catskill delta complex is approximately 3100ft (954m) thick, and can be divided into five lithofacies: black basinal shales; shelf sandstones, siltstones, and shales; shelf siltstones and shales; littoral and fluvio-deltaic sandstones; and red delta-plain shale and sandstone (Fig. 3) (Boswell and Donaldson, 1988).

The Catskill deltaic wedge is divided into numerous chronostratigraphic intervals that provide workable units for stratigraphic correlation (Boswell and others, 1987). These intervals are bounded by regionally correlatable shales that closely approximate time lines. The Elizabeth sandstone is within one of these intervals and consists of upper and lower sandstones. Because the focus of this paper is the upper unit, it will be referred to herein as "the Elizabeth sandstone". Both the Elizabeth and lower Elizabeth sandstones in the vicinity of Elkins are part of the Cannon Hill Formation of the Hampshire Group (Fig. 2) (Boswell and others, 1987).

THE ELIZABETH SANDSTONE IN THE SUBSURFACE

Subsurface Elizabeth sandstone isolith patterns based on mapping of sandstone thicknesses observed in gamma ray logs from oil and gas wells west of the Devonian outcrop belt in West Virginia indicate a generally strike-parallel configuration in the subsurface west of Elkins (Fig. 4a). North and south of the area shown in Figure 4a regional isolith patterns of the Elizabeth sandstone reveal numerous dip-trending patterns (Boswell and Jewell, 1988). A cross section from the Elkins outcrops to the subsurface (Fig. 4b) shows flat-

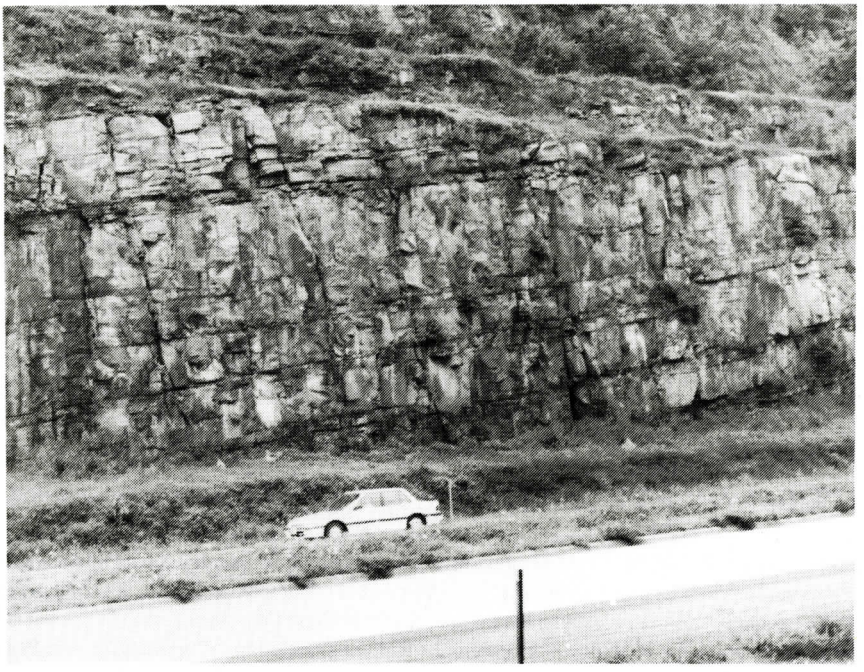

Figure 1: Photograph of the Elizabeth sandstone, showing massive, tabular bedding in lower 30 ft (9.2 m), and thinner tabular bedding in upper 12 ft (3.7 m).

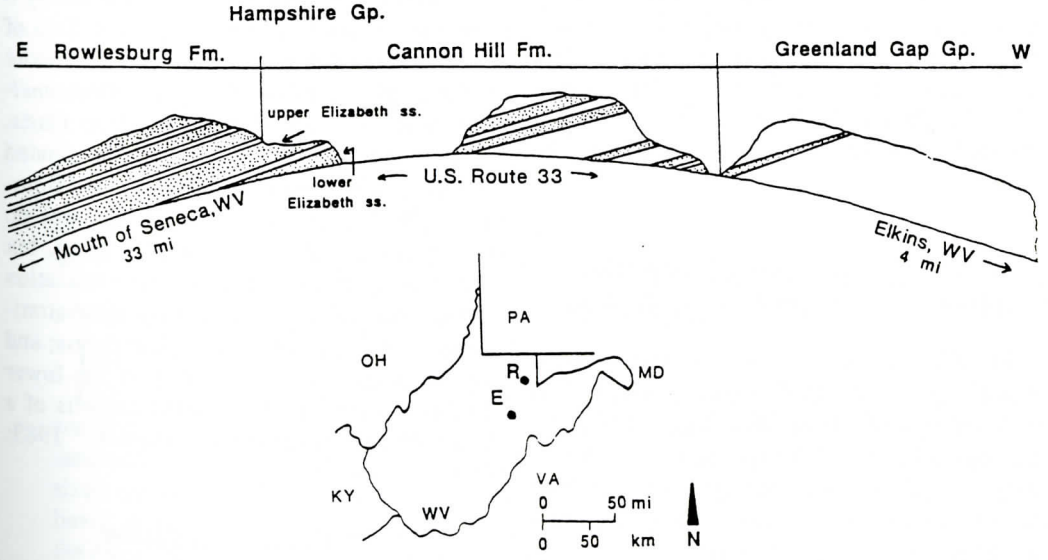

Figure 2: Location of outcrops of the Catskill delta complex on Cheat Mountain, 4 mi (6.4 km) east of Elkins, West Virginia. E=Elkins, R=Rowlesburg.

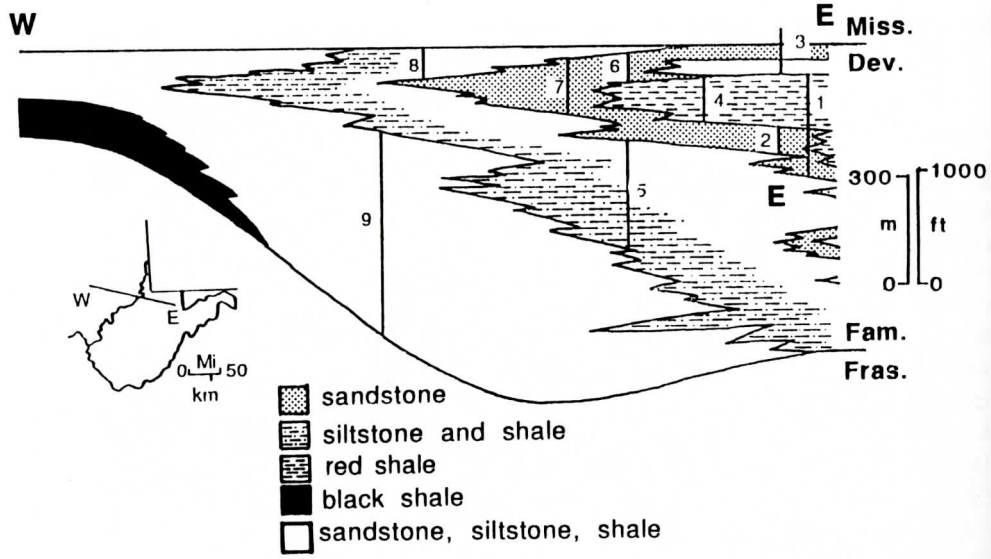

Figure 3: Lithofacies of the Catskill Delta Complex in a cross section from southeastern Ohio to the western edge of the Devonian outcrop belt in east-central West Virginia. 1= Hampshire Group, 2= Cannon Hill Formation, 3= Price Formation, 4= Rowlesburg Formation, 5= Greenland Gap Formation, 6= Oswayo Formation, 7= Venango Formation, 8= Riceville Formation, 9= Brallier Formation (after Boswell and Donaldson, 1988). E= Elizabeth sandstone.

bottomed, blocky gamma ray signatures and westward thinning. Gamma ray signatures of this type suggest pronounced wave reworking (Fisher, 1969) and the strike-parallel orientation suggests locally wave-dominant conditions (Swift and others, 1972). Depositional strike of the Elizabeth sandstone shoreline in the study area was approximately north-northeast.

ELIZABETH SANDSTONE AND ADJACENT UNITS IN OUTCROP

The Elizabeth sandstone is exposed in roadcuts along U.S. Route 33 approximately 4.0 mi (6.4 km) east of Elkins, West Virginia (Fig. 1). Similar facies are also exposed in cliffs along Shavers Fork of the Cheat River one mile from the roadcut exposures. This study is based primarily on the roadcut exposures.

Directly beneath the massive Elizabeth sandstone is a 30 ft (9 m) thick sequence of interbedded shale and sandstone (Fig. 5). The shales are dark brown to dark gray, and contain abundant macerated plant debris and large coalified plant fragments. Some of these larger coaly fragments contain pyrite.

Sandstone beds range from approximately 6 in to 3 ft (14 cm to 1 m) in thickness. Two of the thicker beds contain basal lags of siderite nodules, articulated brachiopods *(Rhynconellida)*, bivalves *(Glossites)*, and shale clasts. Bedding above these lags is finely laminated and hummocky cross-stratified (Dott and Bourgeois, 1982). Most of the thin sandstones do not exhibit distinct internal stratification, but are of a pinch and swell form. This association of large, fossiliferous, hummocky cross-stratified sandstones; shales rich in plant debris; and thin pinch-and-swell sandstones in the lower Elizabeth interval indicate storm deposits of a shallow-shelf environment (Lewis, 1983; McDowell, 1988).

The Elizabeth sandstone

The Elizabeth sandstone in outcrop is approximately 54 ft (17 m) thick. It can be divided into three units on the basis of grain size, sedimentary structures, and bedding thickness. These units are designated, from

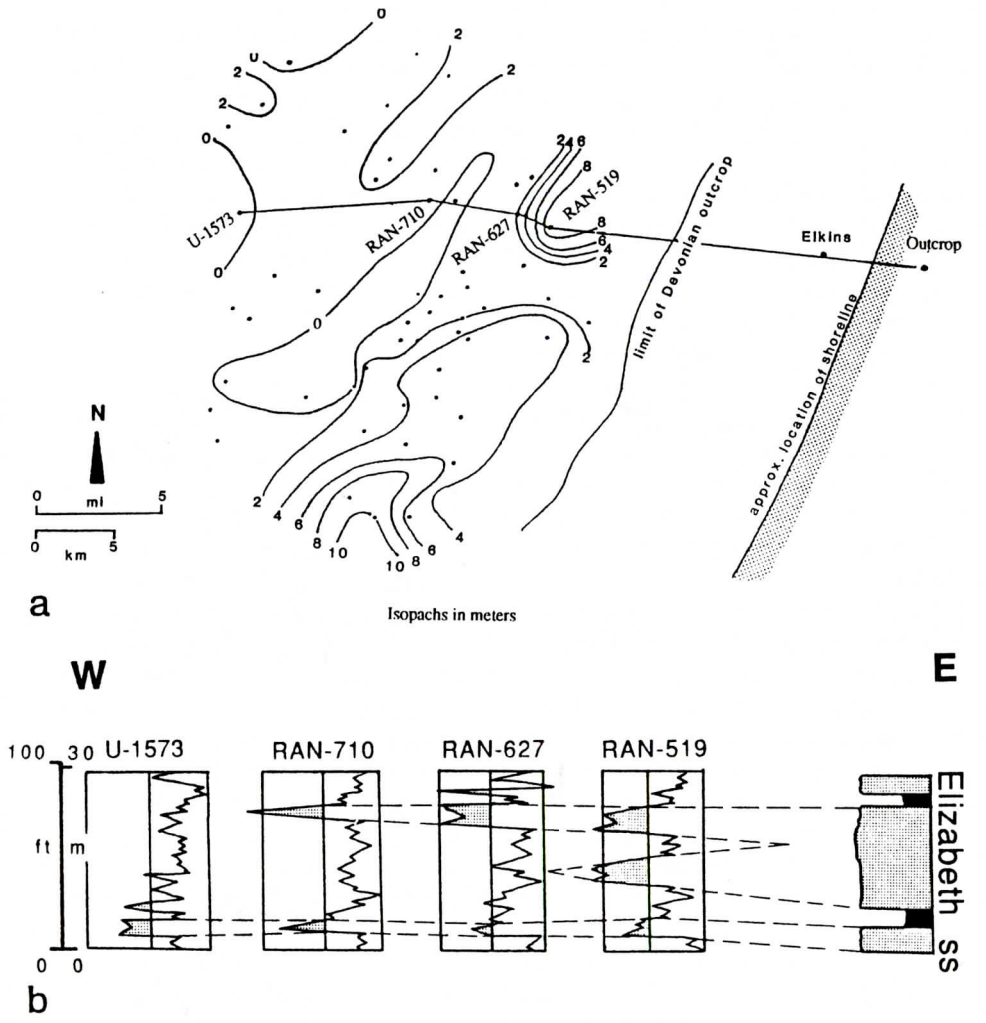

Figure 4: a) subsurface isolith patterns of the Elizabeth sandstone. Contour interval = 2 m. Cross section line shown. b) cross section from the Elkins outcrop to the nearby subsurface.

youngest to oldest, as A, B, and C (Fig. 5).

Unit C

Unit C is approximately 5 ft (16 m) thick and consists mainly of fine- to medium-grained sandstone with scattered, thin lenses of gravel-sized quartz. Bedding is massive and exhibits broad, shallow, trough crossbedding. Overlying the crossbedded sandstone are two beds of horizontally laminated sandstone 16 in (.4 m) and 10 in (0.25 m) thick, each containing basal lags of shale clasts. No fossils are visible in this part of the Elizabeth sandstone, except for scattered *Arenocolites* burrows that extend down from bedding planes.

Unit B

The contact between units B and C is gradational. Unit B is approximately 25 ft (8 m) thick and consists of medium-grained to pebbly sandstone with abundant lenses and stringers of very coarse-grained to granule-sized quartz. The largest pebble diameter measured in this unit is 1.25 in (3.1 cm). Bedding in unit B is massive, and includes a very complex assemblage of sedimentary structures.

Any sedimentary structures that may have existed in the lower five feet of unit B have

been largely obscured by bioturbation. *Skolithos* and *Arenocolites* burrows are abundant. This bioturbated zone is overlain by a crossbedded, very coarse-grained to pebbly sandstone in wedge-shaped bedsets that have an average thickness of approximately 3-4 in (8-10 cm). Sedimentary structures of this size and shape dominate unit B with three notable exceptions (Fig. 5):

1) Approximately 10.0 ft (3.1 m) above the base of the unit a laterally continuous shaly parting overlies large-scale current ripples (dunes) in very coarse-grained sandstone. The dunes have amplitudes of 0.5 in (3.4 cm) and a wavelength of 0.1 ft (3.0 cm). Dune crests trend N12°E, and dune cross-lamination dips to the northwest. Beneath these dunes, other cross-lamination sets indicate multi-directional flow.

2) Directly above the shaly parting that covers the dunes is a large (16 in, 40 cm) bedset of crossbeds in very coarse-grained to gravelly sandstone. Individual crossbeds are tangential and do not appear to show a systematic variation in grain size from top to bottom. The crossbeds, which can be seen in three dimensions, dip uniformly to the northeast. This bedset is overlain by medium scale wedge-shaped crossbed sets that dominate the unit.

3) Approximately 5 ft (1.5 m) above the large tangential crossbeds is a bedset of large-scale trough crossbeds in medium- to coarse-grained sandstone. This trough set is approximately 16 in (0.36 m) thick, and the axis of the trough trends N50°E.

Unit A

Unit A is separated from unit B by a thin shale that is continuous for the length of the outcrop (approx. 800 ft, or 246m). The lower 4 ft (1.2 m) of unit A consists of thin- to medium-bedded, medium- to fine-grained sandstone that exhibits horizontal and subhorizontal lamination, and, in one location, eastward-dipping large-scale planar crossbedding. Bedding planes in this zone are typically micaceous; and thin, discontinuous, rippled shale partings are common. *Arenocolites* burrows are abundant in this interval. A large (20 in, 0.45 m) bedset of trough crossbedding overlies the thin- to medium-bedded zone in medium-grained to pebbly sandstone. Unit A is capped by approximately 5 ft (1.5 m) of medium-grained sandstone which has horizontal and subhorizontal laminations. Bedding is thick to very thick, and shaly partings are rare. Root bioturbation can be seen in the upper few centimeters of the Elizabeth sandstone, and the contact with the overlying shale is sharp.

Units overlying the Elizabeth sandstone

A gray to reddish-gray shale containing the brackish-water brachiopod *Lingula* overlies the Elizabeth sandstone (Fig. 5). Above the shale is a sandstone that has convolute bedding at the base that is directly overlain by a quartz pebble conglomerate with eastward-directed crossbedding. The conglomerate contains articulated *Rhynconellida* and *Glossites*, and trepostome bryozoans. The conglomerate extends the entire length of the outcrop, a distance of 800 ft (246 m), at a constant stratigraphic horizon suggesting a single depositional event. Above the conglomeratic sandstone is a massive, 32 ft (10 m) thick, medium-to fine-grained sandstone that has large, laterally continuous, concave-upward, scour surfaces within the sandstone. These surfaces are marked by lags of quartz pebbles, siderite nodules, and shale intraclasts with a distinctive red color. At the top, the sandstone interfingers with an overlying red shale.

The presence of *Lingula* in the reddish gray shale directly above the Elizabeth sandstone indicate a brackish-water lagoonal environment. The fossiliferous beds are capped by a storm or washover deposit which is represented by the conglomeratic sandstone. The sandstone containing channel lags and scour surfaces represents progradation of a fluvial deposystem over a lagoonal environment. This latter sandstone unit is the lower Bayard sandstone and corresponds to a large-scale offlap noted in the subsurface by Boswell and Jewell (1988) and McDowell (1988).

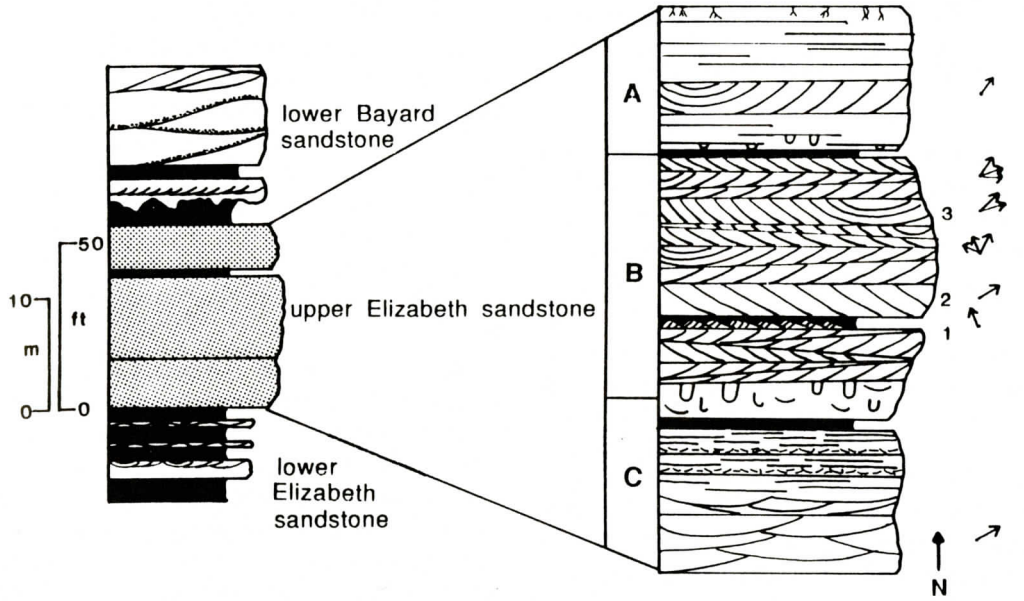

Figure 5: Columnar section of the Elizabeth sandstone and associated units, showing sedimentary structures and subintervals. Numbers next to right-hand column refer to structures described in text. Arrows indicate paleocurrent directions.

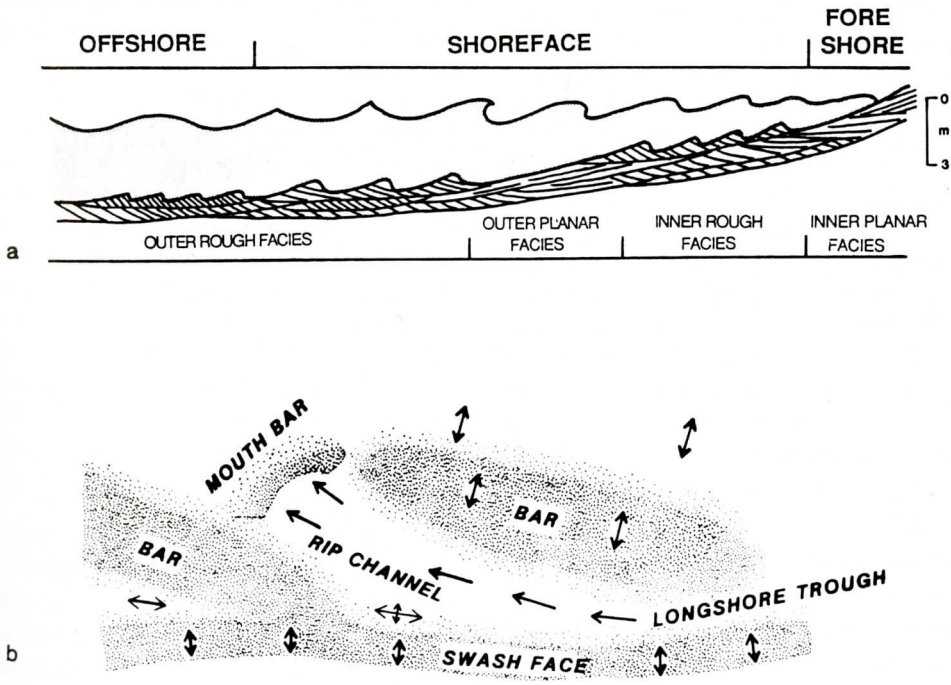

Figure 6: a) Shoreline-parallel facies belts of the shoreface and foreshore zone in non-barred systems. Bedforms not to scale (from Clifton and others, 1971); b) Morphology of foreshore and shoreface zones complicated by oblique bar, longshore trough, and rip channels. These subenvironments occur within the inner rough facies. Arrows indicate direction and relative magnitude of oscillatory or unidirectional flow (from Hunter and others, 1979).

MODELS OF NEARSHORE DEPOSITION AND GENERAL CHARACTERISTICS OF THE ELIZABETH SANDSTONE

The dominant processes affecting sediment dispersal and deposition in the nearshore environment are longshore currents, rip currents, tidal currents, and waves. In the foreshore environment this situation is modified by the presence of swash bars.

The nearshore environment can be subdivided into three zones: offshore, shoreface, and foreshore. Clifton and others (1971) have further subdivided the shoreface and foreshore into shore-parallel "facies belts" on basis of wave-generated bedforms. These are: outer rough, outer planar, inner rough, and inner planar (Fig. 6a). In the lower shoreface (the outer rough facies), net onshore wave oscillation causes the formation of lunate and straight-crested dunes of low amplitude and landward-directed planar or shallow trough crossbedding. In shallower water, these bedforms are either washed out or do not form because of upper flow regime conditions, resulting in the plane bed configuration of the outer planar facies. In the surf zone (the inner rough facies), waves break and travel landward as a wave bore, producing complex bedforms that indicate dominantly landward current directions. Finally, flow up and down the swash face creates the plane bed of the inner planar facies. The facies belts may migrate as a function of wave energy and tides, but in nearshore environments uncomplicated by the presence of offshore bars (a non-barred system) the relative position of the zones is invariable (Clifton and others, 1971).

A nearshore environment that is similar to the non-barred system of Clifton and others (1971), but with nearshore bars is described by Hunter and others (1979). Most of the nearshore bars are connected to the beach and extend seaward oblique to the shoreline (Fig. 6b). Between the bars and the swash face are longshore troughs that parallel the shoreline and bend seaward into rip channels. In the longshore trough, current flow is dominantly parallel or oblique to the shore as reflected in the orientation of dunes. Dunes that form in rip channels are dominantly seaward facing, but this is complicated by onshore wave oscillation at different tide levels and wave regimes. At the seaward end of the rip channels, small mouth bars are deposited and are covered with dominantly seaward-facing dunes. During low tide, these dunes may be partially washed out by waves, resulting in upper-flow-regime plane bed.

The combination of onshore-directed wave oscillation, longshore currents, and offshore-directed rip currents operating over a complex shoreface morphology results in a complex assemblage of sedimentary structures. In a regressive shoreline environment these structures should occur in a predictable sequence with respect to lower shoreface and foreshore structures (Clifton and others, 1971).

Figure 7 summarizes the predicted sedimentary structures, subenvironments, and hydrodynamic processes in regressive barred and non-barred nearshore systems. Table I also presents the succession of sedimentary structures in the Elizabeth sandstone. Four observations are important: 1) The Elizabeth sandstone exhibits a succession of sedimentary structures analogous to the outer rough, outer planar, inner rough, and inner planar facies of both modern examples. 2) The most complex assemblage of sedimentary structures of the Elizabeth sandstone are coincident with the coarsest grain size, as in both barred and non-barred modern systems. 3) The large-scale trough and planar crossbeds in the coarse to pebbly zones of the Elizabeth sandstone are very similar to those described by Hunter and others (1979), who attributed them to relatively strong unidirectional or strongly asymmetric oscillatory flow in barred nearshore systems. 4) The Elizabeth sandstone is overlain by fluvial and washover sandstone and overlies marine-fossil bearing shale and sandstone.

INTERPRETATION

The Elizabeth sandstone, which overlies

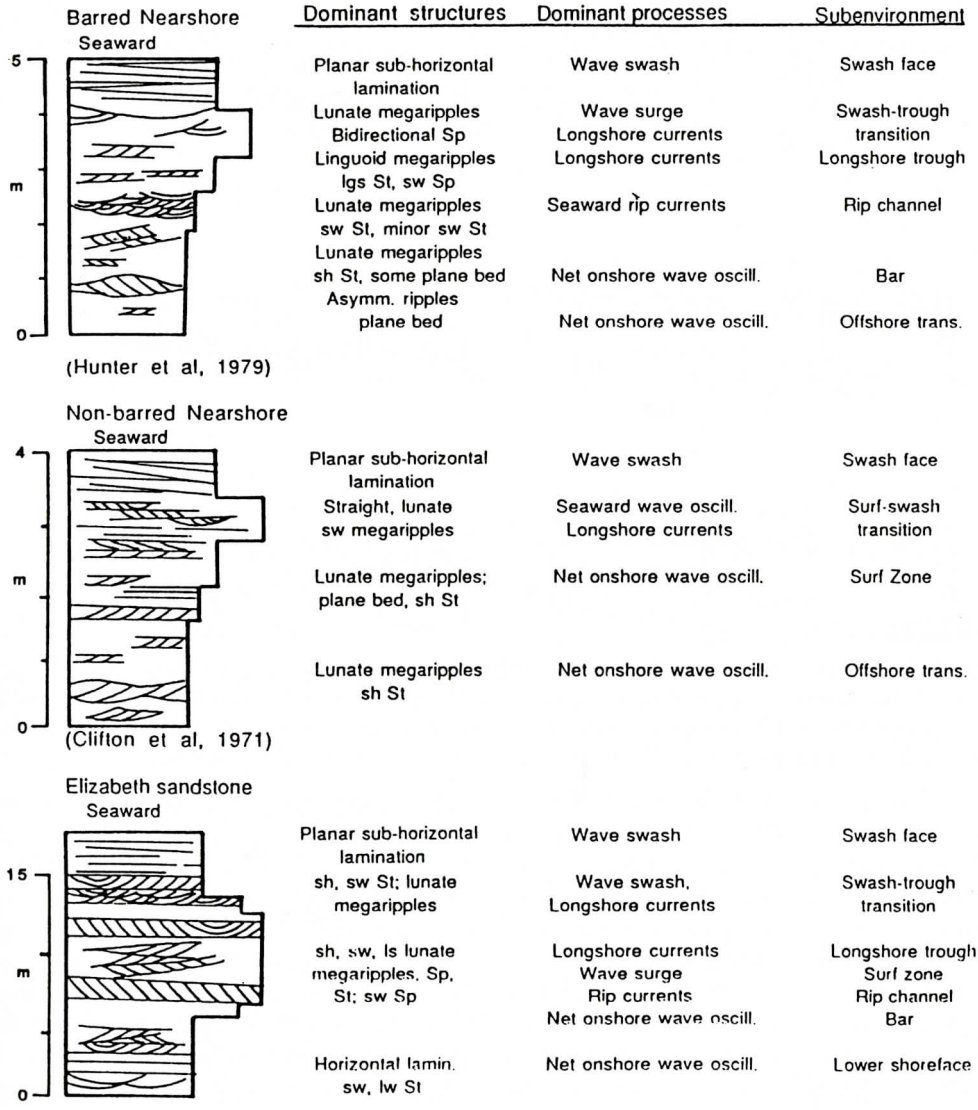

Figure 7. Comparison of sedimentary structures, hydrodynamics, and subenvironments of deposition for non-barred and barred shorelines, and the Elizabeth sandstone. Sp = planar crossbeds, St = trough crossbeds, lgs = longshore, sh = shoreward, sw = seaward.

shelf deposits of the lower Elizabeth interval and is overlain by lagoonal and fluvial deposits of the lower Bayard sandstone, is in the appropriate stratigraphic position for a regressive shoreline deposit. The Elizabeth sandstone exhibits a sequence of sedimentary structures reflecting deposition in a regressive shoreline setting, i.e. progressively shallower and higher-energy environments, as is documented in Figure 7.

Unit C of the Elizabeth sandstone represents deposition in lower to upper shoreface environments. Broad, shallow trough- crossbedding overlain by horizontally laminated sandstone is typical of the outer rough and outer planar facies. Storm influence is indicated by the units directly below the Elizabeth sandstone.

Unit B of the Elizabeth sandstone was deposited in the upper shoreface environment. As the specific hydrodynamics, morphology,

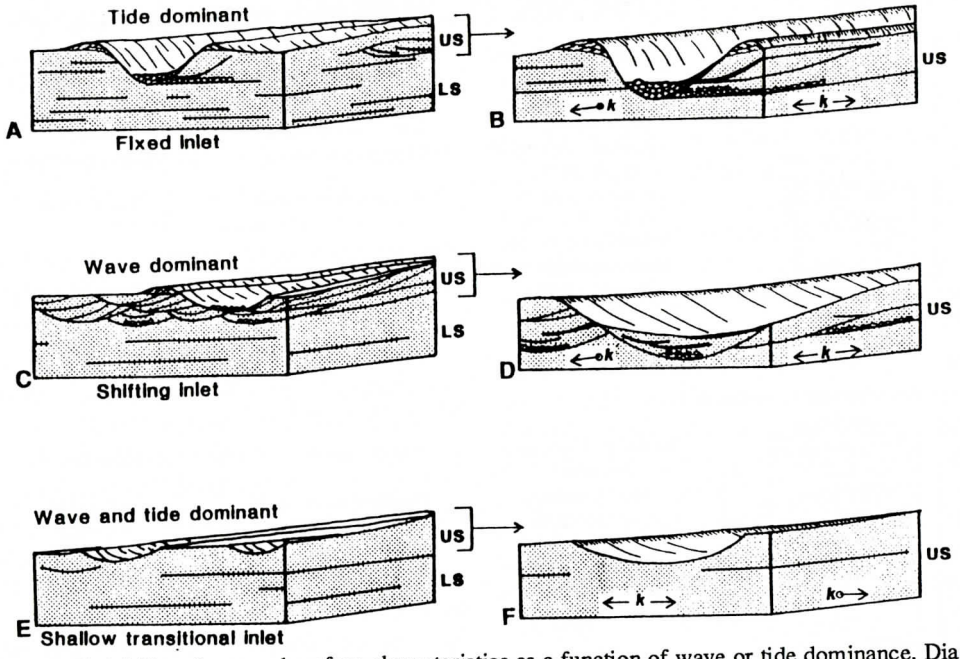

Figure 8. Variability of upper shoreface characteristics as a function of wave or tide dominance. Diagrams a,c, and e show upper and lower shoreface geometries. Diagrams b,d, and f show details of tidal-inlet fill. US = upper shoreface; LS = lower shoreface; k = permeability, arrows indicate principal directions of permeability (after Hubbard and others,1979; Galloway,1986; and Tyler and Ambrose,1986).

and location of the shoreface subenvironments may vary widely with changing conditions such as wave energy, tides, and storms (Hunter and others, 1979), it may not be possible to accurately identify the specific subenvironments in the Elizabeth sandstone. However, the dominance of multidirectional, but dominantly shoreward-directed, medium-scale crossbedding (Fig. 5) reflects the complex interaction in the upper shoreface of onshore wave oscillation, seaward or oblique rip currents, and longshore currents. In this context, the large, eastward-directed planar crossbed set probably represents landward migration of a large sand wave or swash bar as a result of landward-directed wave oscillation. The large, northeast-directed, trough crossbed set may reflect lunate dunes formed in a rip channel or longshore trough.

Foreshore deposition is represented by unit A. The horizontal and sub-horizontal lamination that comprises most of this zone is typical of swash-zone deposition. Landward-directed planar crossbedding associated with rippled shaly partings suggests a local ridge-and-runnel environment rather than a high-energy longshore trough (Davis and others, 1972). A longshore trough is indicated by the deep trough crossbed set (axis trends N10°E) in unit A. The relative abundance of argillaceous sediment in the lower four feet of unit A is somewhat problematic. The fine grain size may reflect either a greater input of mud and silt from a nearby sediment dispersal source or a local decrease in wave energy.

Numerical models of the Catskill sea (Slingerland, 1986) indicate that the Devonian shoreline in West Virginia was probably mesotidal to low macrotidal, and thus would be expected to show some evidence of strong tidal influence. The typical spacing of tidal inlets on tide-dominant coastlines is far greater than the width of the outcrops discussed here; however, the lack of channel-fill deposits in the Elizabeth sandstone at Elkins suggests that tidal inlet migration was not extensive. This seems contradictory to models of wave-dominant barrier systems in which wave-induced longshore

currents cause inlets to migrate in a down-current direction. The sedimentary structures described here do indicate strong wave energy, suggesting that tidal inlets of the Elizabeth sandstone barrier island may have been transitional in character between deeply entrenched, stable inlets of a tide-dominant system and rapidly shifting, unstable inlets of a wave-dominant system. Transitional inlets of this type are widely-spaced, have large width/depth ratios, and have variable channel characteristics (Hubbard and others, 1979). The Elizabeth sandstone may thus reflect a balance between high wave energy and strong tidal currents.

Deltaic facies are found in outcrops of the Elizabeth sandstone approximately 30 miles (50 km) to the north along depositional strike at Rowlesburg, WV (Fig. 2). Boswell and Jewell (1988) have mapped large depocenters of Elizabeth sandstone in the subsurface 10 miles (16 km) north of Rowlesburg and approximately 15 miles (25 km) south of Elkins. The high volume of sandstone at Elkins is probably a result of a prolific sediment source from one or both of these nearby delta systems, suggesting that the Elizabeth shoreline exposed at Elkins represents a delta margin or interdeltaic barrier. It also indicates that dispersive wave energy was high.

EFFECT OF DEPOSITIONAL ENVIRONMENT ON RESERVOIR CHARACTERISTICS

Because inlets may have been widely spaced and shallow during deposition of the Elizabeth sandstone, permeability barriers that would be created by abundant inlet fill, such as mud drapes on accretionary bedding and slack water mud drapes in the channel bottom, may be insignificant in the Elizabeth sandstone and sandstones of similar origin. Indeed, the only significant shale breaks seen in outcrop are bedding-parallel and would act as permeability barriers only to vertical flow. Because the facies belts of a barred shoreface are parallel to the shoreline, reservoirs in barred shoreface sandstones would likely be characterized by permeability trends parallel to depositional strike rather than compartmentalized by deep, widely spaced or numerous, closely spaced inlet-fill deposits transverse to depositional strike.

Figure 8 shows block diagrams through the centers of different barrier island models based on varying degrees of wave, tide, and fluvial dispersion of sediment. The principal differences with respect to permeability barriers are the spacing and thickness of tidal inlet and ebb tidal delta deposits. In the example of tide-dominant shorelines, entrenched tidal inlets provide permeability trends and barriers transverse to the barrier island core (Fig. 8a). This may be complicated by the occurrence of slack water mud drapes on channel margins and on ebb tidal delta surfaces (Fig. 8b). Figure 8c depicts a wave-dominant system with numerous, closely-spaced inlet-fill deposits. Ebb tidal deltas would be small and lacking in mud because of wave energy, but the numerous channel-fill deposits could act to significantly complicate permeability due to the presence of channel-bottom mud drapes or channel lags (Fig. 8d). Extensive migration of these inlets could result in a very heterogeneous reservoir. The Elizabeth sandstone is most similar to Figure 8e, in which wave and tidal energy are balanced to produce compositionally mature sands between widely-spaced, shallow inlets. Ebb tidal deltas would also be relatively mud-free. The result would be a reservoir with permeability directions parallel to depositional strike uncomplicated by transverse shale breaks (Fig. 8e).

CONCLUSIONS

The Elizabeth sandstone is interpreted to represent a nearshore deposit of a barred, high-energy, wave- and tide-dominant system affected by strong longshore and offshore-directed rip currents. This interpretation is made on the basis of: 1) the stratigraphic position of the Elizabeth sandstone between subjacent shelf deposits and superjacent lagoonal and fluvial sandstones; 2) a sequence of sedimentary structures that indicates progressively

shallower water and higher energy conditions; 3) sedimentary structures very similar to those observed in modern, high-energy shoreline sands; and 4) a lack of tidal inlet-fill deposits. The three subdivisions of the unit represent deposition in, from bottom to top, the lower to upper shoreface where net landward wave oscillation caused the development of broad, shallow trough crossbedding and plane beds (unit C); lower foreshore environment where strongly asymmetric landward wave oscillation, longshore currents, and rip currents created a complex assemblage of trough and planar cross beds (unit B); and the upper foreshore or swash face where wave swash caused the development of upper-flow-regime plane bed (unit A).

The entire Catskill sea was interpreted by Slingerland (1986) to have been high mesotidal to low macrotidal; however, the lack of tidal-channel-fill deposits in the Elizabeth sandstone near Elkins and the sedimentary structures diagnostic of high wave energy indicate that tidal inlets of the Elizabeth shoreline between the adjacent depocenters did not migrate extensively, and may have been widely spaced and shallow. Permeability barriers associated with tidal inlet fill deposits are probably scarce in the shoreface parts of the Elizabeth sandstone near Elkins, meaning that principal reservoir permeability is parallel to depositional strike. Some subsurface shoreline sandstones of the Catskill delta complex and other hydrocarbon-producing areas interpreted as resulting from wave dominance may have the hybrid characteristics of the Elizabeth sandstone and thus exhibit similar strike-parallel, outcrop-scale permeability trends.

ACKNOWLEDGEMENTS

This paper is expanded from part of an M.S. thesis done at West Virginia University under the direction of Alan C. Donaldson, to whom I am grateful for his guidance during completion of the thesis. I am also grateful to W. A. Thomas and A. W. Shultz for their helpful comments and suggestions on this manuscript. Editorial comments by Ray Boswell, and John Dennison greatly improved the manuscript. Field work for this project was funded partially by the Chevron Field Fund administered by West Virginia University.

REFERENCES CITED

Boswell, R.M., Donaldson, A.C., and Lewis, J.S., 1987, Subsurface stratigraphy of the Upper Devonian and Lower Mississippian of northern West Virginia: Southeastern Geology, v. 28, p. 105-131.

Boswell, R.M., and Jewell, G.A., 1988, Atlas of Upper Devonian/ Lower Mississippian sandstones in the subsurface of West Virginia: West Virginia Geological and Economic Survey, Circular C-43, 143 p.

Boswell, R.M., and Donaldson, A.C., 1988, Depositional architecture of the Acadian clastic wedge of the central Appalachian Basin, U.S.A., *in* McMillan, N.J., Embry, A.F., and Glass, D.J., eds., Devonian of the world: Canadian Society of Petroleum Geologists Memoir 14, p. 65-84.

Boswell, R.M., 1988, Basin analysis of the Acadian clastic wedge in northern West Virginia and adjacent areas [Ph.D. thesis]: West Virginia University, Morgantown, WV, 351 p.

Clifton, H.E., Hunter, R.E., and Phillips, B.L., 1971, Depositional structures and processes in the non-barred high-energy nearshore: Journal of Sedimentary Petrology, v. 41, p. 651-670.

Coleman, J.M., 1976, Deltas: Processes of deposition and models for exploration: Continuing Education Publishing Company, Champaign, Illinois, 102 p.

Coleman, J.M., and Prior, D.B., 1982, Deltaic environments of deposition, *in* Scholle, P.A., and Spearing, D., eds., Sandstone Depositional Environments: American Association of Petroleum Geologists Memoir 31, p. 139-178.

Davis, R.A., Jr., Fox, W.T., Hayes, M.O., and Boothroyd, J.C., 1972, Comparison of ridge and runnel systems in tidal and non-tidal environments: Journal of Sedimentary Petrology, v. 32, p. 413-421.

Davis, R.A., Jr., and Clifton, H.E., 1987, Sea-level change and the preservation potential of wave-dominated and tide-dominated coastal sequences, *in* Nummedal, D., Pilkey, O.H., and Howard, J.D., eds., Sea-level fluctuation and coastal evolution: Society of Economic Paleontologists and Mineralogists Special Publication no. 41, p. 167-180.

Dennison, J.M., 1971, Petroleum related to Middle and Upper Devonian deltaic facies in the central Appalachians: American Association of Petroleum Geologists Bulletin, v. 55, p. 1179-1193.

Dennison, J.M., 1985, Catskill, Delta shallow marine strata, *in*Woodrow, D.L., and Sevon, W.D., eds., The Catskill Delta: Geological Soci-

ety of America Special paper 201, p. 91-106.
Dott, R.H., and Bourgeois, J., 1982, Hummocky stratification: Significance of its variable bedding sequences: Geological Society of America Bulletin, v. 93, p. 663-680.
Ettensohn, F.R., 1985, The Catskill Delta complex and the Acadian Orogeny: A model, *in* Woodrow, D.L., and Sevon, W.D., eds., The Catskill Delta: Geological Society of America Special Paper 201, p. 39-50.
Fisher, W.L., 1969, Facies characterization of Gulf Coast Basin delta systems with some Holocene analogues: Transactions of the Gulf Coast Association Geological Society, v. 19, p. 239- 261.
Fisher, W.L., and McGowen, J.H., 1969, Depositional systems in Wilcox Group (Eocene) of Texas and their relation to occurrence of oil and gas: American Association of Petroleum Geologists Bulletin, p. 30 - 54.
Galloway, W.E., 1986, Reservoir facies characteristics of microtidal barrier systems: American Association of Petroleum Geologists Bulletin, v. 70, p. 787-808.
Hubbard, D.K., Oertel, G., and Nummedal, Dag, 1979, The role of waves and tidal currents in the development of tidal-inlet sedimentarystructures and sand body geometry: Examples from North Carolina, South Carolina, and Georgia: Journal of Sedimentary Petrology, v. 49, p. 1073-1092.
Hunter, R.E., Clifton, H.E., and Phillips, R.L., 1979, Depositional processes, sedimentary structures, and predicted vertical sequences in barred nearshore systems, southern Oregon coast: Journal of Sedimentary Petrology, v. 49, p. 711-726.
Lewis, S., 1983, Reservoir rocks of the Catskill Delta in northern West Virginia: Stratigraphic basin analysis emphasizing deposition [M.S. thesis]: West Virginia University, Morgantown,WV, 148 p.
McCubbin, D.G., 1982, Barrier-island and strand plain facies, *in* Scholle, P.A., and Spearing, D.R., eds., Sandstone Depositional Environments: American Association of Petroleum Geologists Memoir 31, p. 247-280.
McCubbin, D.G., and Brady, M.J., 1969, Depositional environments of the Almond reservoirs, Patrick Draw field, Wyoming: The Mountain Geologist, v. 6, p. 3-26.
McDowell, R.J., 1988, Depositional environments of the Upper Chemung and Lower Hampshire Formations [M.S. thesis]: West Virginia University, Morgantown, WV, 168 p.
Slingerland, R.L., 1986, Numerical computation of co-oscillating paleolatitudes in the Catskill epeiric sea of North America: Sedimentology, v. 33, p. 487-497.
Swift, D.J.P., Holliday, B., Avignone, N., and Shideler, G., 1972, Anatomy of a shoreface ridge system, False Cape, Virginia: Marine Geology, v. 12, p. 59-84.
Tyler, N., and Ambrose, W.A., 1986, Facies architecture and production characteristics of strandplain reservoirs in North Markham - North Bay City Field, Frio Formation, Texas: American Association of Petroleum Geologists Bulletin, v. 70, p. 809-829.

SOUTHEASTERN GEOLOGY
V. 33, No. 1, October 1992, p.37-51

GRAVITY AND MAGNETIC MODELING OF THE DUNBARTON TRIASSIC BASIN, SOUTH CAROLINA

R. J. CUMBEST[1]
Dept. of Geological and Geophysical Sciences, Princeton University
Princeton, NJ 08544

VAN PRICE
Environmental Monitoring Section,
Building 773-57A, Westinghouse Savannah River Co.
Aiken, S.C. 29808

ERIC E. ANDERSON
Department of Geological Sciences,
University of South Carolina
Columbia, S.C. 29208

ABSTRACT

A model of the Dunbarton extensional basin is presented in which the gravity and magnetic anomalies are modeled simultaneously. The model is constrained by core from 36 drill holes, transient electromagnetic, and seismic data. It is shown that the geometry and extent of the Dunbarton basin can be determined from the gravity data after the interference from mafic bodies has been excluded.

INTRODUCTION

Many fault-bounded, elongate depositional basins occur along the eastern coast of North America (Froelich and Olsen, 1984). These basins contain mafic volcanics and sediments as old as Late Triassic (Carnian) and are associated with the crustal thinning and rifting phase of North American Atlantic continental margin development. The basins occur as relatively narrow, trough-like structures in the Piedmont, and some are partially to completely covered by Coastal Plain sediments. Gravity and magnetic modeling, ideally complemented by drill core, are potentially useful geophysical techniques for resolving the structure and geometry of the basins covered by Coastal Plain sediments.

The gravity and magnetic anomalies associated with Mesozoic extensional basins along the North American Continental margin are highly variable. This variability is presumably due to the presence of both high density, high magnetic susceptibility mafic rocks and low density, low magnetic susceptibility sedimentary rocks. The magnetic signature can range from anomalous highs over the basin (Bain and Harvey, 1977), to anomalous lows (Marine and Siple, 1974), to no response at all (Hanson, 1988). The gravitational response is less varied but is still not straightforward in that in some cases no gravity low is present and where anomalous gravity lows are found their magnitude is sometimes not sufficient to account for the relatively low density sedimentary fill (Bell and others, 1988). A 15-20 mgal gravity high is associated with the hanging wall of the structural units that form some of these basins. Bell and others (1988) noticed that this gravity high is typically composed of two features: relatively short wavelength (50 km), approximately 25 mgal "inner gravity high" that occurs just to the east of the basin, and a broader (100 km) 20 mgal "outer gravity high" further to the southeast. Although, the "outer gravity high" sometimes appears to merge with the "inner gravity high". This variable geo-

1. Current address: Environmental Monitoring Section, Westinghouse Savannah River Co., Aiken, SC 29808.

physical signature is attributed to the presence of mafic rocks both within and near the basins, resulting in localized magnetic anomalies (Sumner, 1977) and a mass excess (Bell and others, 1988). The interference produced by these mafic rocks complicates detailed modeling of individual basin structure and geometry. Simultaneous modeling of the gravity and magnetic anomalies can significantly reduce this problem since use of both magnetic and gravity modeling may provide additional constraints on the system (Guspi and Introcaso, 1988).

DUNBARTON BASIN

The Dunbarton Triassic basin beneath the Coastal Plain of South Carolina coincides with both a gravity and magnetic low. The general extent and shape of the Dunbarton basin was originally presented by Marine and Siple (1974) based on core from wells that penetrated approximately 350 m. of Coastal Plain sediments, and from an aeromagnetic contour map (Petty and others, 1965) in conjunction with a limited amount of seismic data. Marine and Siple (1974) attributed the anomalous magnetic low to greater depths to crystalline magnetic basement rock beneath the basin. They also noted a major change in the nature of the metamorphic basement to the south. Since sediments in the basin have a very low magnetic susceptibility, the magnetic signal from high magnetic susceptibility rocks to the south

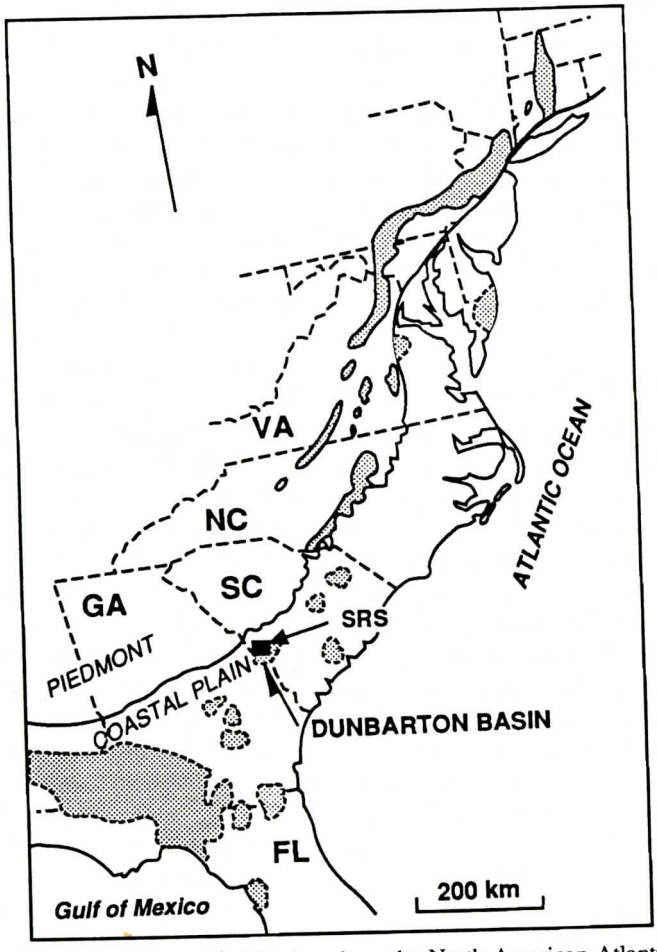

Figure 1. Location of Mesozoic extensional basins along the North American Atlantic margin. Savannah River Site and Dunbarton Triassic basin indicated (adapted from Marine and Siple, 1974).

of the basin may potentially obscure or dominate the magnetic signature of the basin itself and therefore make delineation of the basin geometry from magnetic data alone imprecise.

This study presents the results of simultaneous modeling of gravity and magnetic data, with constraints provided both by drill core, seismic refraction, and transient electromagnetic data. This modeling will demonstrate that the magnetic signature alone is poorly suited to detailed modeling of the basin geometry due to interference from surrounding mafic bodies.

GEOLOGIC SETTING AND GEOLOGIC CONTROL

The Savannah River Site (SRS) occurs in the Coastal Plain of South Carolina adjacent to the Savannah River, approximately 20 miles southeast of the nearest exposure of the Piedmont - Coastal Plain unconformity (Figure 1). The Dunbarton basin underlies the southeastern half of SRS where the Coastal Plain sequence increases in thickness from approximately 200 m to the northwest of SRS to over 350 m to the south.

The Piedmont exposed northwest of the Coastal Plain in this region (Maher, 1979; Secor and others, 1986; Secor, 1987) consists of amphibolite facies gneisses and schists of the Kiokee Belt to the northwest separated by the Augusta fault from a sequence of greenschist facies volcanic and volcaniclastic rocks (Belair Belt). The Kiokee belt and the tectonic boundary between the Kiokee belt and Belair belt is intruded by variably deformed, late

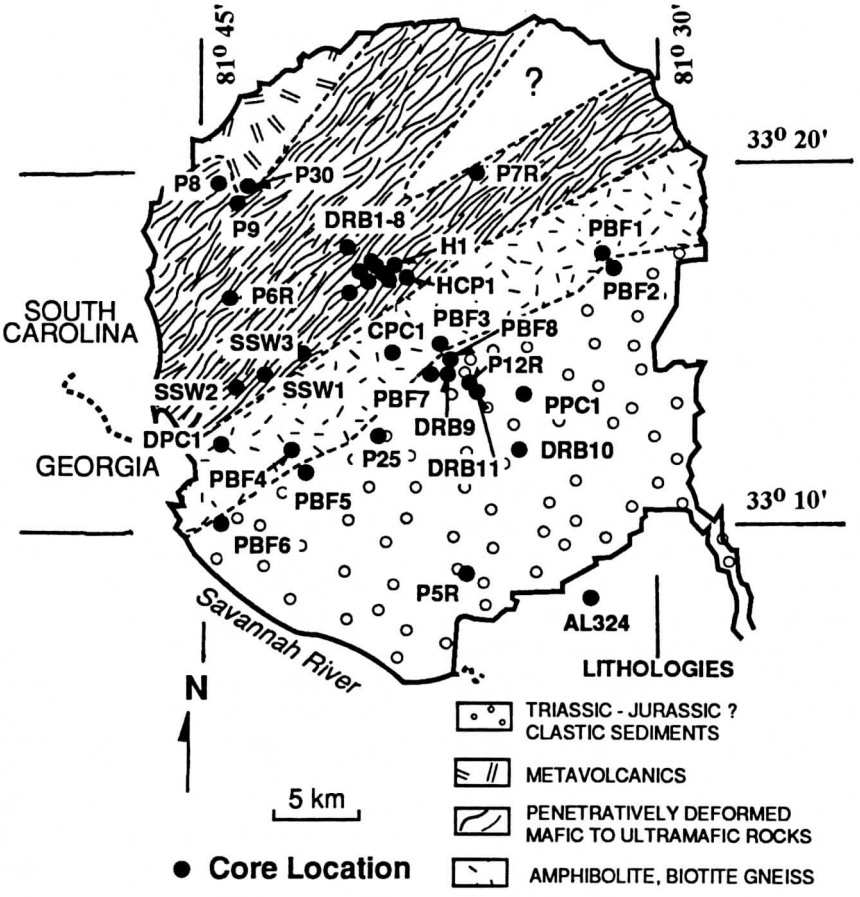

Figure 2. Sub-Coastal Plain geologic map of SRS with the location of wells that recovered drill core from the Piedmont beneath SRS indicated.

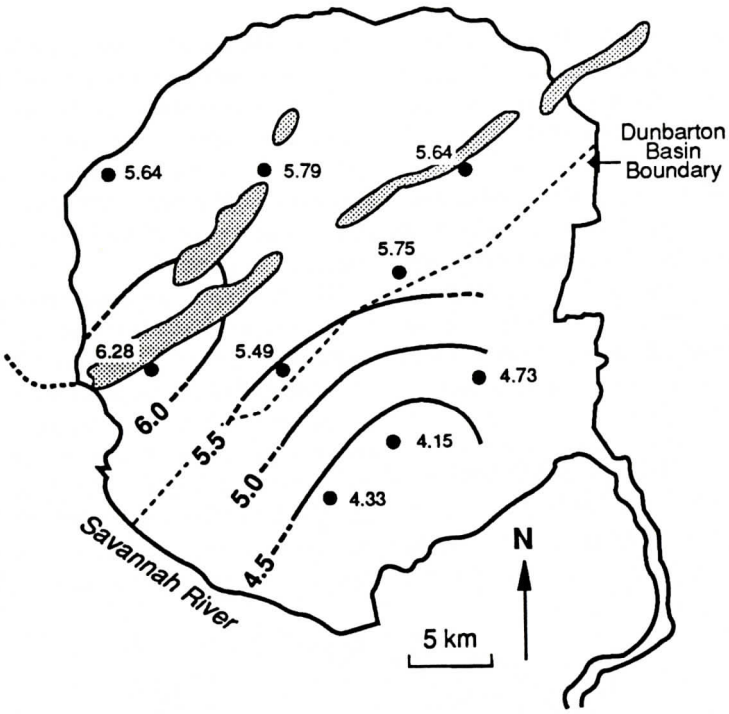

Figure 3. Seismic refraction velocities (kms^{-1}) from the Piedmont beneath the SRS. Approximate location of boundary between crystalline basement and Dunbarton basin indicated. Magnetic highs shaded.

Paleozoic (Dallmeyer and others, 1986) granitic plutons.

Information concerning the sub-Coastal Plain geology beneath SRS is derived primarily from drill core. The location of wells that have recovered core from the basement beneath the Coastal Plain and the associated lithologies are illustrated on Figure 2. Several wells (DRB9, DRB10, DRB11, P5R, P12R, PCP1, P25, PBF2, PBF5, PBF6, PBF7, and PBF8) recovered immature, clastic sediments that are associated with the Dunbarton basin. These sediments are assumed to be Triassic - Jurassic? in age based on their similarity to sediments found in other Triassic basins (Marine and Siple, 1974). Well DRB-9 penetrated approximately 490 m of clastic sediments before passing into deformed granodiorites in the basement. North of the wells that intersect Triassic sedimentary rocks wells DRB1-8, SSW1-3, HPC1, H1, P6R, P7R, P8, P9, CPC1, PBF1, PBF3, and PBF4 did not intersect any Triassic rock. These wells show that the Triassic sequence is missing in this area. Rocks from these wells are quartz-feldspathic schists, gneisses, amphibolite, hornblende - chlorite schists, metagabbro, and serpentinite, some of which record penetrative mylonitic and cataclastic fabrics indicating the presence of metamorphic rocks with felsic, mafic, and ultramafic protoliths. These rocks show lithologic and metamorphic characteristics more similar to those of the higher grade Kiokee Belt than those of the lower grade Belair Belt. At least one well, P30, recovered greenschist grade metavolcanics indicating that rocks similar to the Belair belt are present beneath the northern part of SRS. This implies that some sort of tectonic boundary is present in the basement separating the greenschist metavolcanic terrain from the amphibolite facies terrain. Structure contour mapping (Westinghouse Savannah River Co., 1989) of the Piedmont - Coastal Plain interface based on these wells indicate that this surface is essentially flat on a regional scale with a gentle southeast slope and very little topographic relief.

The sparse distribution of the few wells that

sampled the sub-Coastal Plain Piedmont can provide only a spotty picture of the geology beneath SRS, but extrapolation of the geology between wells and to other parts of SRS is provided in a general sense by previous geophysical studies. A seismic reflection - refraction survey by CONOCO sampled basement (sub-Coastal Plain) velocities in several locations (Figure 3). Refraction velocities for Piedmont and Triassic rocks have previously been determined by Bonini and Woollard (1960) and are presented in Table 1. Bonini and Woollard (1960) saw no significant difference in gneiss, schist, and granite refraction velocities, although the mafic rocks and Triassic sediments show distinctive differences. As can be seen from Figure 3 the lower velocities consistent with Triassic lithologies are found in the southern part of SRS and can be correlated very well with wells that recovered Triassic rocks. The closest constraint on the Piedmont - Triassic contact is provided by well pairs PBF1 - PBF2, PBF3 - PBF8, and PBF4 - PBF5. The Piedmont - Triassic contact as determined from these wells is very close to the interpolated location of the 5.4 km/sec. refraction velocity contour (Figure 3) consistent with the data of Bonini and Woollard (1960). Seismic refraction data also indicate a pronounced elongate area of velocities greater than 6.0 km/sec. in the northern part of SRS (Figure 3). These refraction velocities are consistent with the presence of mafic rocks and this is confirmed by wells recovering core from this area.

Although the CONOCO seismic reflection survey did not image the Triassic basin, a band of multiple event reflections are present that dip approximately 25 degrees southeast and project to the Piedmont - Coastal Plain interface in the northern part of SRS. The locality where these reflectors project is coincident with the elongate area of high velocities determined from the refraction data (Figure 3). Based on the occurrence of rocks with penetrative strain in drill core from this area and the presence of a distinctive magnetic lineament these reflectors have been previously interpreted to be a fault in the Piedmont with a complex, poly-deformational history. This fault has been associated with the extensional development of the Dunbarton Triassic basin.

A transient electromagnetic survey (TEM) of SRS has also placed constraints on the general extent and depth of the Dunbarton Basin. Figure 4 shows depth to resistive basement for SRS as determined by the TEM survey. Interpretation of TEM data is sensitive to the choice of an initial depth-resistivity model. Where well control is available to provide an initial model, results are quite good. There are no wells to establish model constraints for the entire thickness of the Triassic rocks. Therefore we consider the estimate of depth to basement within the basin to be no better than +/- 10 percent.

Table 1. Seismic Refraction Velocities for Piedmont Rocks (from Bonini and Woollard, 1960)

Lithology	Velocity (km/sec)
gneiss, schist, slate, granitic rocks	5.4
mafic rocks	6.8
Triassic sediments	3.7

MAGNETIC DATA SET

Figure 5 shows an aeromagnetic contour map of SRS and surrounding area. This is a portion of a total intensity aeromagnetic contour map produced by Petty and others (1965). Data collection for this map was accomplished with northwest - southeast flight lines 1 mile apart and 500 ft. above the ground.

Several general features can be seen on the aeromagnetic data. A subelliptical shaped, -200 nT, northeast trending magnetic low occurs in the southern part of SRS. As previously discussed, this area generally coincides with the Dunbarton Triassic basin as determined from drill core and seismic refraction velocities. Immediately southeast of this magnetic low is a magnetic high region composed of several

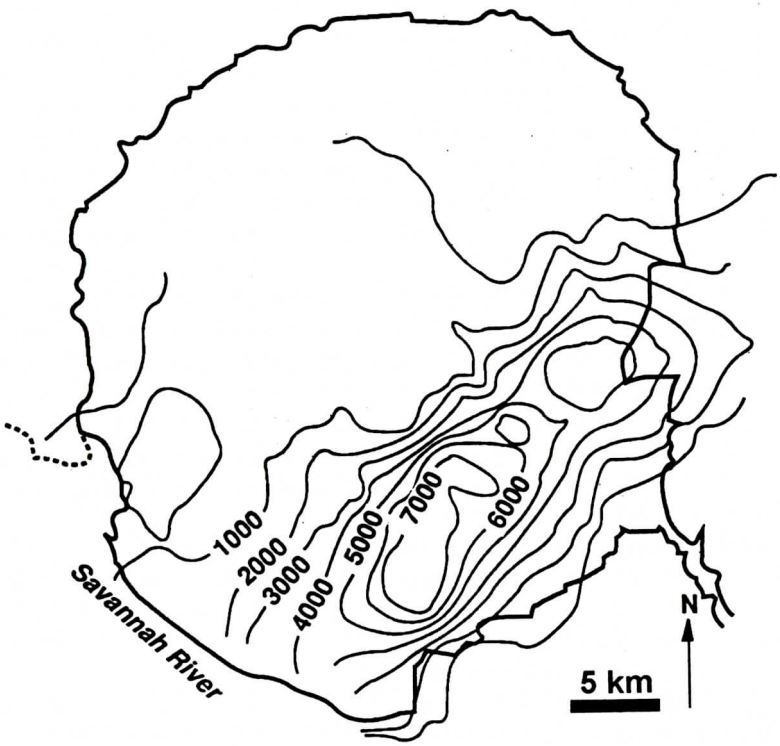

Figure 4. Contoured depth (ft) to resistive basement for SRS as determined by transient electromagnetic survey.

closely spaced elongate to circular magnetic highs, some of which have amplitudes of 1500 nT. These magnetic highs are associated with gravitational highs and have previously been interpreted as mafic intrusions (Daniels, 1974; Daniels and others, 1983). Along the northern edge of the subelliptical magnetic low over the Dunbarton Triassic basin is a northeast - southwest trending magnetic lineament. This lineament is defined by several elongate, 300 nT magnetic highs and associated magnetic lows that form a narrow, linear magnetic anomaly. Based on seismic refraction velocities and drill core the magnetic highs can be associated with the presence of metamorphosed mafic and ultramafic rocks. As discussed previously this magnetic lineament has been interpreted as a fault in the Piedmont and correlated with the Eastern Piedmont fault system and the extensional development of the Dunbarton Triassic basin. The occurrence of magnetic lows on the northwestern side of the lineament are consistent with southeast dipping magnetic bodies.

For modeling purposes 3 northwest - southeast transects across SRS and surrounding areas (Figure 5) were digitized at 0.5 km intervals. This orientation was chosen because it was perpendicular to the strike of all the features of interest in the model.

GRAVITY DATA SET

Gravity data for this study (Figure 6) were compiled from three sources. A ground magnetic and gravity survey was conducted as part of the Dunbarton Basin study reported by Marine and Siple, 1974. A regional line in this study extended from approximately the center of SRS to Fairfax, South Carolina, 50 km to the southeast. A second source is the simple Bouguer anomaly map of South Carolina (Talwani and others, 1975). A third source is a detailed gravity survey conducted by Anderson (1990).

The gravity data show features that can be

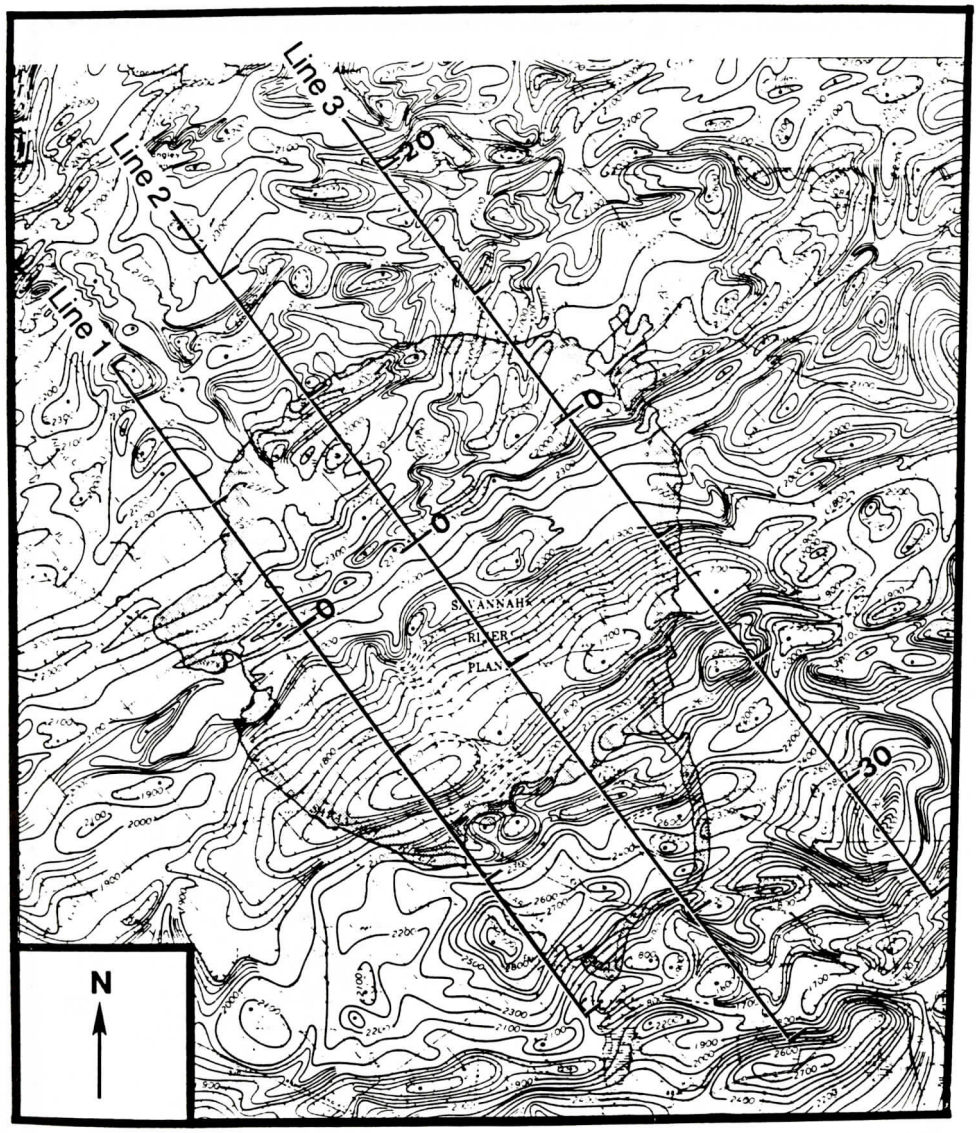

Figure 5. Total intensity aeromagnetic contour map of SRS and surrounding area (adapted from Petty and others, 1965). Locations of magnetic profile lines used for modeling indicated. Distance along lines indicated in kilometers.

generally associated with previously discussed magnetic anomalies. An elongate low approximately -5 to -10 mgal occurs in the location of the Dunbarton Triassic basin. The minimum in the gravity data occurs to the northwest of the minimum in the corresponding magnetic low. Southeast of the Dunbarton basin gravity low, a 10 - 15 mgal gravity high occurs in association with the magnetic high seen in this area. As mentioned previously, this is probably indicative of mafic intrusions. In the east central part of SRS, in proximity to the previously discussed magnetic lineament; several short-wavelength (0.5 - 1.0 km) anomalous areas occur as indicated by the sinuous nature of the gravity contours. This short-wavelength behavior in the gravity data indicate relatively shallow sharp density gradients and are probably

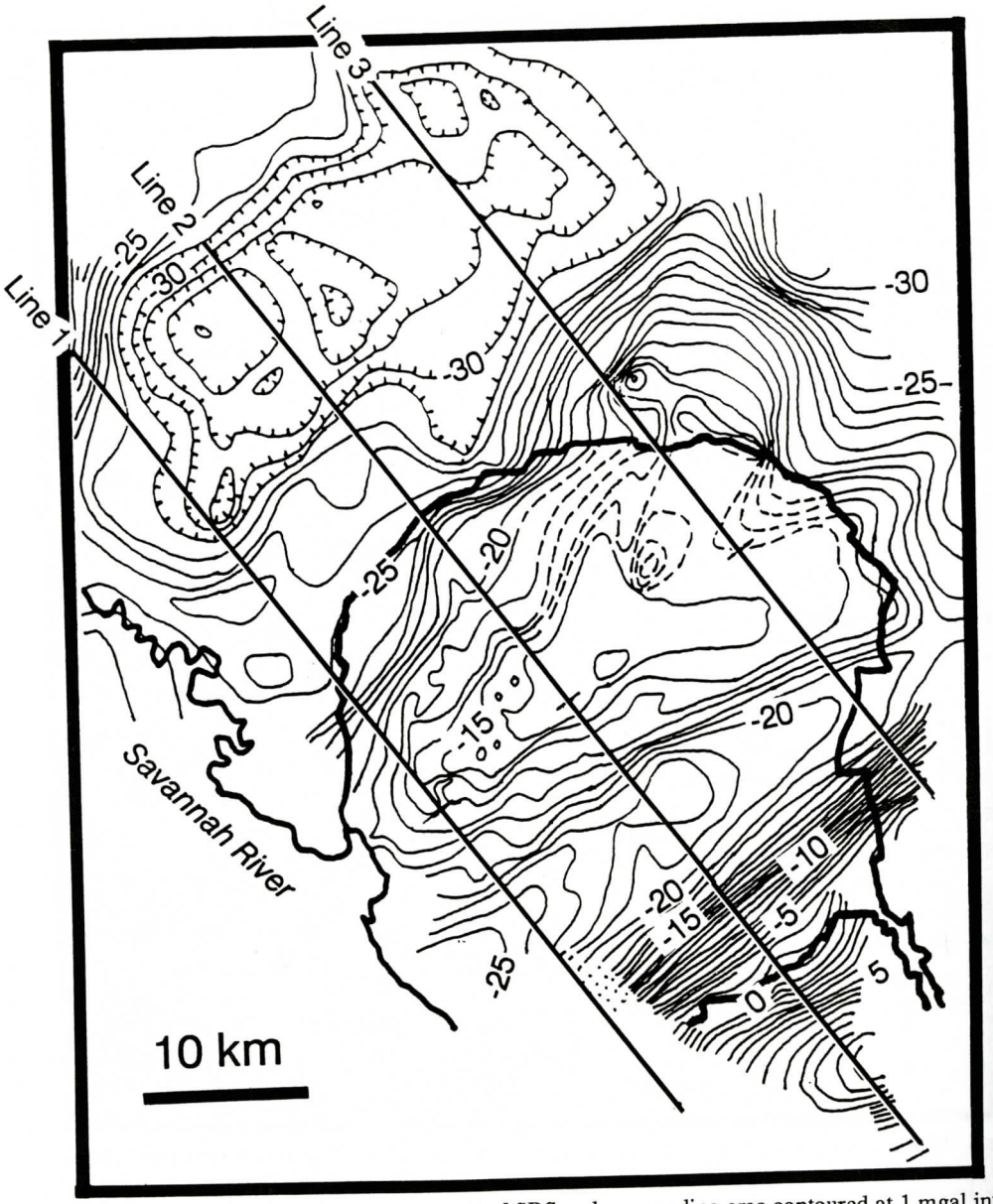

Figure 6. Simple Bouguer gravity anomaly map of SRS and surrounding area contoured at 1 mgal interval. Locations of gravity profile lines used for modeling indicated. From Anderson, 1990.

associated with the metamorphosed mafic bodies that produce the elongate magnetic highs in this area. The gravity data show a distinct -10 to -15 mgal gravity low north of SRS that is not clearly associated with any characteristic magnetic feature. Wells recovering core or cuttings from this area indicate that the gravity low corresponds to a monzogranite pluton (Daniels, 1974; Speer, 1982).

For the model, 3 northwest - southeast trending transects were digitized at 0.5 km intervals from the gravity contour map. These transects were in the same location as those used for the magnetic data.

MODELING METHOD AND PARAMETER SELECTION

Gravity and magnetic modeling was done with the program MAGIX produced by INTERPEX Limited. The program utilizes a 2.5 dimension model. The geologic model is input to the program as simple geometric shapes with a given strike length and density or magnetic susceptibility. The program will then calculate the resulting gravity or magnetic profile that is placed symmetrically along the top of the model so that it can be compared with the actual data. An inversion capability is also provided that will make a least squares adjustment to the model to improve the fit of the computed profile to the data.

The input parameters for the magnetic model are the inclination and intensity of the Earth's magnetic field and the magnetic susceptibilities of the various lithologies represented in the model. The value used for the inclination of the Earth's magnetic field was 65 degrees (Dobrin, 1960) and the intensity was 55,000 nT (Dobrin, 1960).

Table 2. Magnetic Susceptibilities for Selected Lithologies

Lithology	Susceptibility (emux 10^{-6})	Susceptibility Contrast
"country rock"	1000	0
metamorphose d mafic rocks	2100	0.0011
monzogranite	400	-0.0004
Triassic Sediments	100	-0.0009
mafic intrusions	7000	0.006

Susceptibilities for the various lithologies used in the model are presented in Table 2. These values were obtained from Daniels (1974), who made bulk susceptibility measurements on rocks from beneath SRS and in the nearby Piedmont and from Sumner (1977). It should be noted that modeling was done in terms of calculated anomalies so that susceptibility contrasts were used as program input. Therefore, it was necessary to assume a "background" susceptibility that would correspond to the country rock containing the various geologic bodies modeled. Drill core from SRS indicates that this "country rock" is highly variable in nature and ranges from quartzofeldspathic schist and gneiss to amphibolite. The value chosen for the background susceptibility was therefore taken intermediate to the susceptibilities of these lithologies.

Table 3: Densities for Selected Lithologies

Lithology	Density (gm/cm^3)	Density Contrast
"county rock"	2.75	0.00
metamorphosed mafic rocks	2.80	0.05
monzogranite	2.65	-0.10
Triassic sediments	2.53	-0.22
mafic intrusions	3.00	0.25
Coastal Plain sediments	2.00	-0.75

For the gravity model, in addition to the geologic model, densities for the various geologic bodies were necessary inputs. The densities used are presented in Table 3. The density chosen for the monzogranite is from analysis of the nearby Springfield granite which is similar in composition and probably consanguineous to the pluton considered in this study (Speer, 1982). Densities for the Triassic clastic rocks and other lithologies were averaged from measurements made on drill core from SRS. Again, the gravity modeling was done in terms of density contrasts so the "background" density was obtained by a similar means. The gravity regional is essentially flat in this area (Talwani and others, 1975).

The lack of significant magnetic susceptibility and low density of the sediments in the

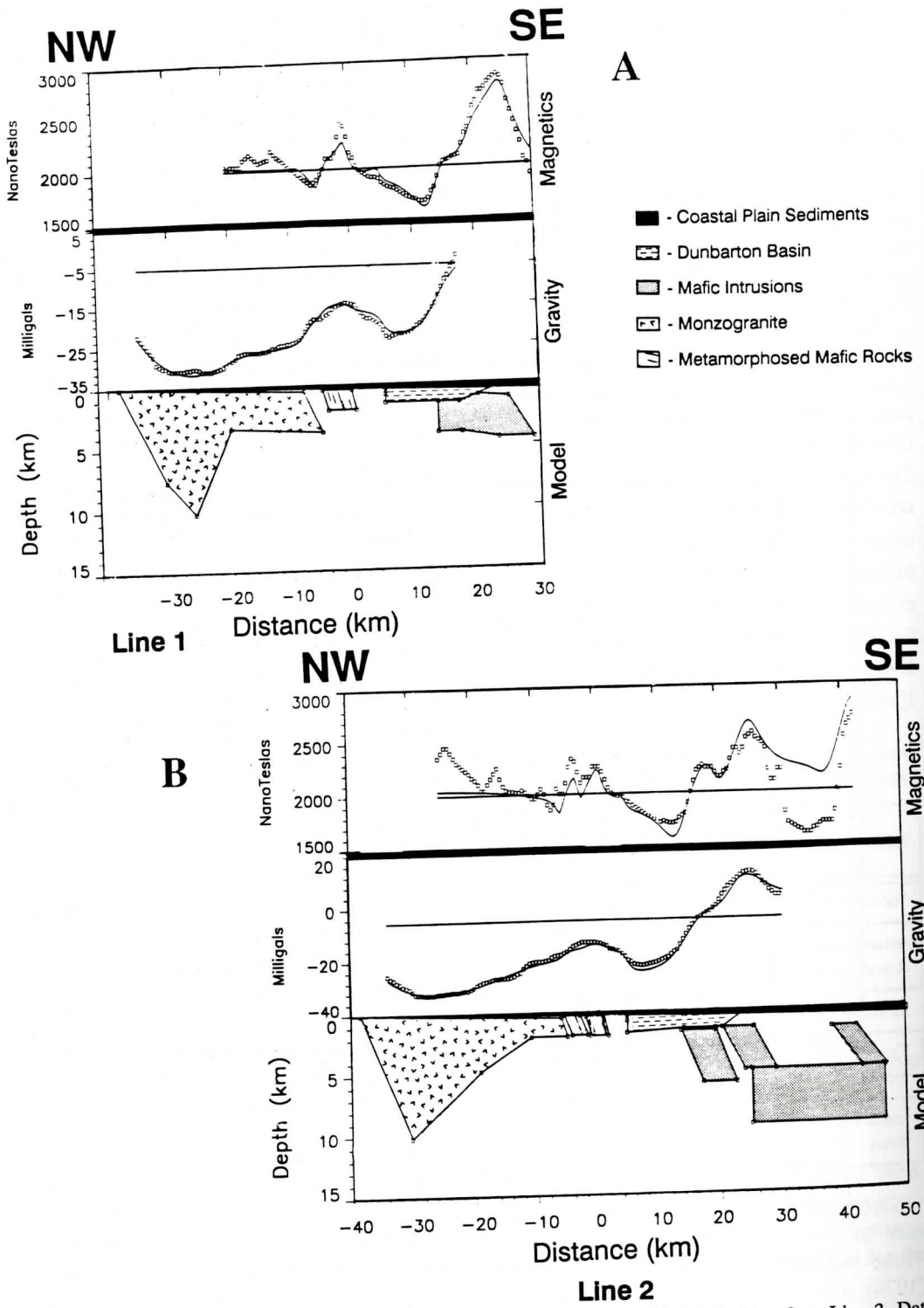

Figure 7. Gravity and magnetic model for SRS and surrounding area. a. Line 1. b. Line 2. c. Line 3. Data indicated by squares. Calculated model indicated by solid line.

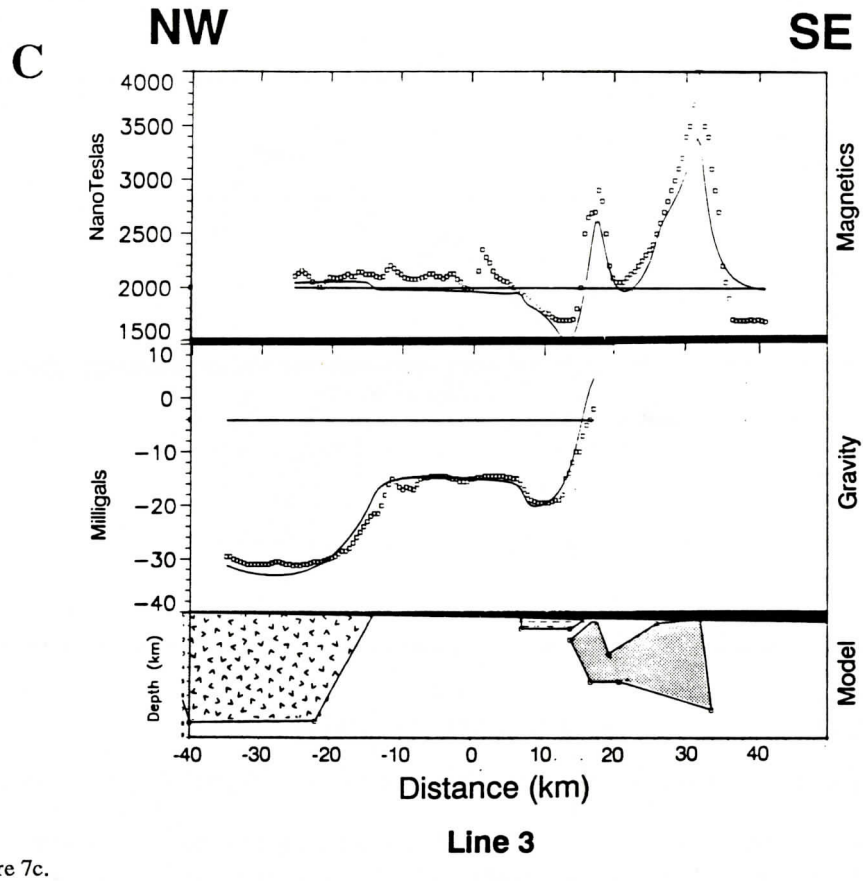

Figure 7c.

Coastal Plain section and the fact that it forms a relatively uniform cover to the basement means that the Coastal Plain will have little effect on the basement anomalies except for the increased distance due to their thickness, but the Coastal Plain section is included in the model as a wide wedge shaped body for completeness.

THE MODEL

Figure 7 compares the geologic model with data for the three chosen profiles. The monzogranite pluton on the northern end of the lines is constrained primarily on the basis of its associated gravity low because it does not have any distinctive magnetic signature. However, there are some short wavelength magnetic variations associated with the pluton. These variations may be due to the presence of mafic enclaves and dikes, or more likely localized concentrations of magnetite which occur as an accessory mineral in the pluton (Speer, 1982).

The contact between the granite pluton and "country rock" inferred from the model occurs in the same location as the postulated fault previously discussed. It is possible that this is a tectonically modified intrusive contact and that the acoustic impedance contrast associated with the contact may give rise to the reflection events seen on the seismic record. The presence of localized magnetic highs in this area also constrain the locality of metamorphosed mafic to ultramafic bodies associated with the fault.

On the southeast ends of the profiles, the gravity and magnetic highs constrain the mafic intrusive bodies. These bodies appear to have a large vertical extent and occur very close to and beneath the southern margin of the Triassic

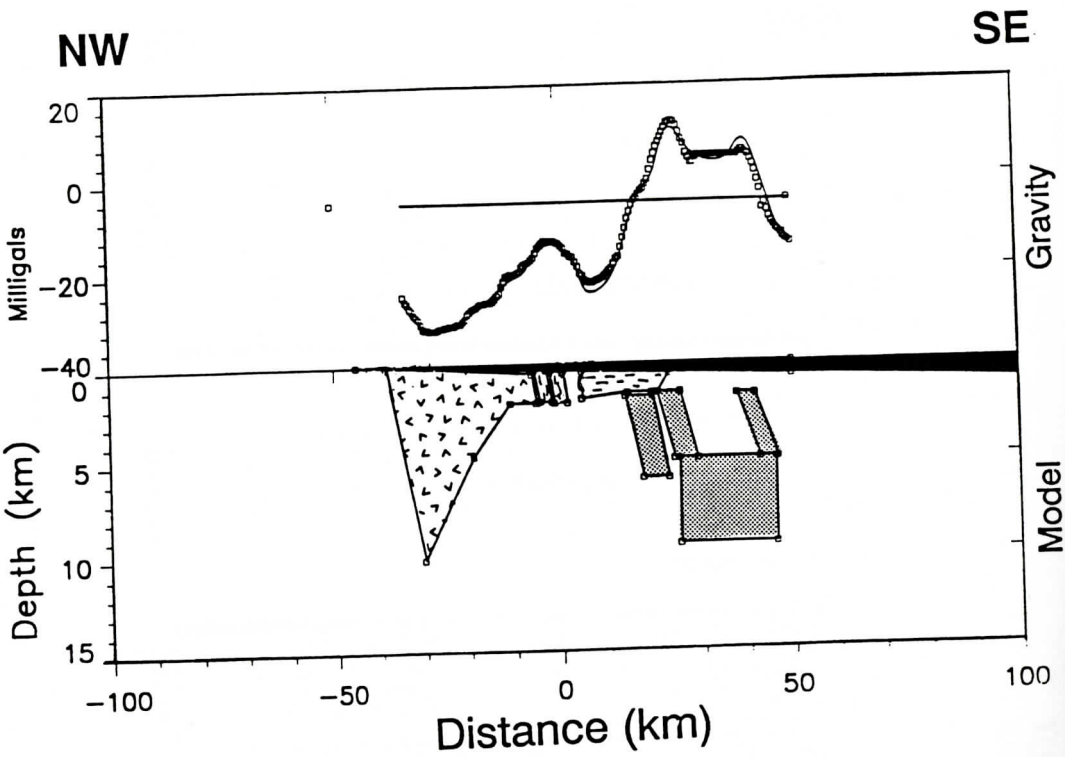

Figure 8. Gravity data and model for the southerly extension of line 2. See Figure 7 for key to lithologies.

basin. On Line 2 (Figure 7b) near the plus 40 km location, the magnetic data reveal a magnetic low that is not reflected by the model. The aeromagnetic contour map (Figure 5) shows that in this area large along-strike gradients occur in the magnetic data. The 2.5 dimensional nature of the modeling program is unsuited for accounting for these along-strike variations, but the gravity data for the southerly extension of Line 2 (Figure 8) requires that a high density body underlie this area.

The size and shape of the Dunbarton basin is based mainly on well control and the results of the transient electromagnetic survey. Figure 9 shows the magnetic and gravity profiles due only to the Triassic basin with the Coastal Plain included. As Figure 9 shows, the basin produces a negligible magnetic signature. As the sedimentary fill is basically non-magnetic, the small signature is entirely due to the "hole" created by the basin resulting in greater distances from the magnetic basement to the datum flight line. The low-density sediments in the basin are capable, however, of producing a significant gravity low of 15 mgal.

Figure 10 shows the magnetic and gravity profiles due to the mafic intrusive body to the southeast of the basin with the Coastal Plain included. As Figure 10 illustrates, a large part of the magnetic low previously associated with the basin is a result of the dipole nature of the magnetic field associated with these intrusive bodies. This effect occurs because any vertical or southeast dipping magnetic body at this latitude will have an associated magnetic low on the northwestern side.

DISCUSSION

As figure 9 and 10 illustrate, the Dunbarton basin is capable of producing a significant gravity anomaly. However, the magnetic anomaly of the Dunbarton Triassic basin is not reliable for use in detailed modeling of the basin location, geometry or extent. This signature is relatively insignificant compared to the mag-

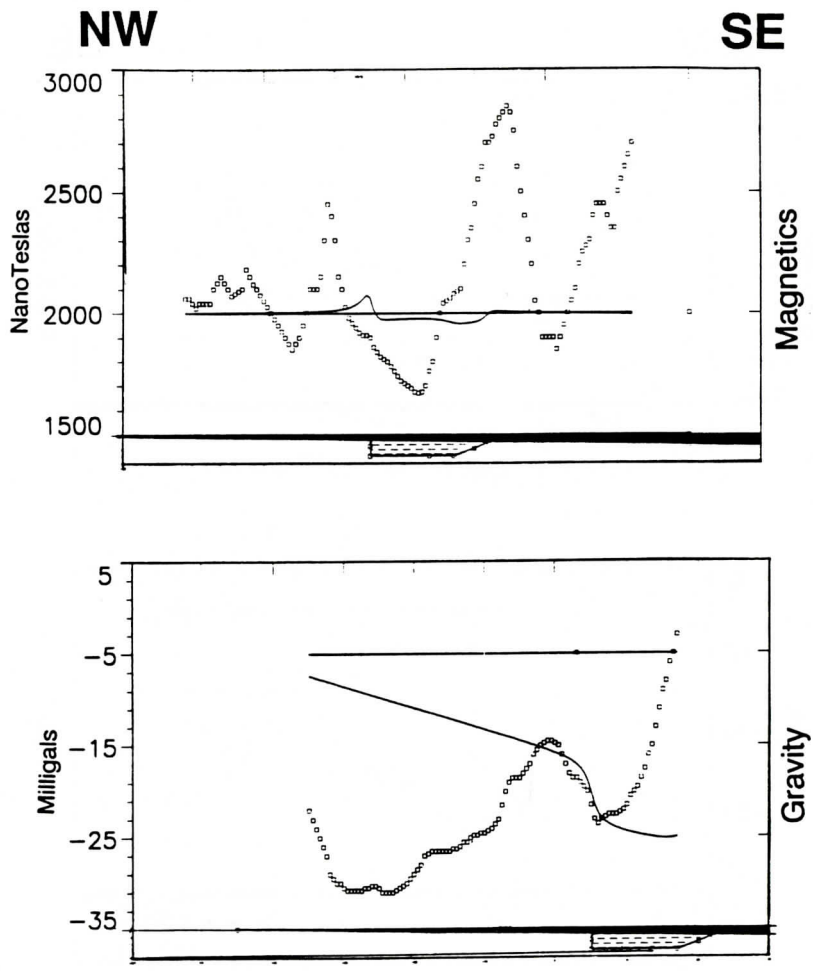

Figure 9. Gravity and magnetic signature of the Dunbarton Basin. Solid line represents basin model anomaly only. See Figure 7 for key to lithologies.

netic lows produced by the mafic intrusions immediately to the southeast, but it should be noted that there may be some genetic relationship between the location and shape of the mafic bodies and the basin geometry and structure. That is, if the mafic bodies are associated with Paleozoic mafic magmatism in the Piedmont, then their presence and rheological properties may have controlled the location and geometry of the basin bounding faults. If on the other hand, the mafic bodies are the same age or younger than the basin, then the faulting associated with basin development may have exerted some control on the intrusions by acting as magmatic conduits as suggested by Bell and others. (1988). These two possibilities could be tested by determining the intrusive age of the mafic lithologies. What is clear, however, from the detailed modeling presented in this manuscript, is that mafic intrusions are closely associated with the southeastern margin of the Dunbarton Triassic basin to produce an "inner gravity high". Gravity models for theoretical basins produced by simple shear of the crust by Bell and others (1988) are very similar in general (Figure 9) to those presented in this manuscript for the Dunbarton Triassic basin. The coincidence of magnetic and gravity anomalies allows us to confirm the presence of mafic rocks in one of the critical areas of the

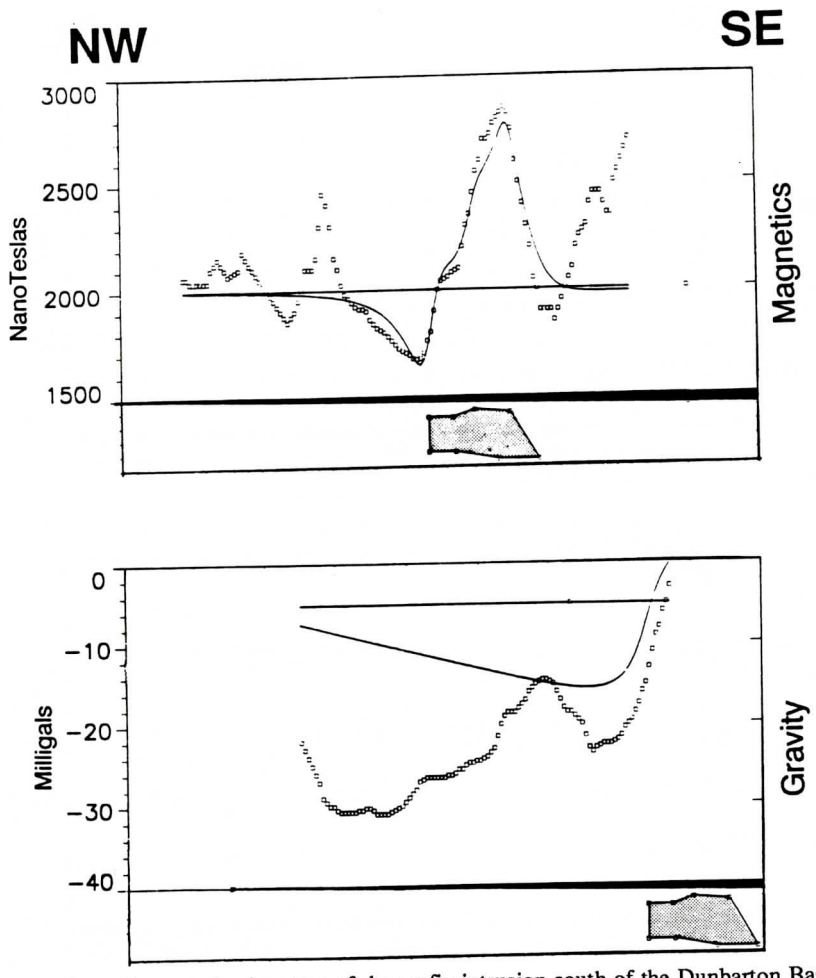

Figure 10. Gravity and magnetic signature of the mafic intrusion south of the Dunbarton Basin. Solid line represents basin model anomaly only. See Figure 7 for key to lithologies.

simple shear model.

CONCLUSIONS

1. Simultaneous, detailed gravity and magnetic modeling, constrained by geologic data from drill core in addition to transient electromagnetic and seismic refraction data is a powerful technique for extrapolating the geometry, structure and location of extensional basins covered by Coastal Plain sediments. However, as demonstrated, magnetic modeling alone is poorly suited for this purpose because the basin signature is relatively minor relative to nearby mafic bodies whose signatures overwhelm that produced by the basins.

2. Low density basin sedimentary fill can produce a significant gravity response, which, when modeled with that produced by the mafic bodies whose presence and size are determined by magnetic modeling, can be used to constrain the thicker parts of the basin.

3. Mafic intrusive bodies are closely associated with the southeastern margin of the Dunbarton Triassic basin. The presence of mafic rocks in this locality is consistent with the simple shear basin development model of Bell and others (1988).

ACKNOWLEDGMENTS

This manuscript has been improved by reviews provided by Pradeep Talwani, Michael Steckler, and Robert D. Hatcher Jr.of the SRS Earth Sciences Advisory Committee.The final version also benefited from suggestions by David Daniels and Carl Burgess. The work was supported under contract DE-AC09-88SR18035 by the U.S. Dept. of Energy, however, the interpretations are those of the authors and do not necessary represent the views of DOE.

REFERENCES

Anderson, E. E., 1990, Seismotectonics of the Savannah River Site: The results of a detailed gravity survey [M.S. Thesis]: Columbia, South Carolina, The University of South Carolina.

Bain, G.L. and Harvey, B.W., 1977, Field guide to the Geology of the Durham Triassic basin: Carolina Geological Society, Fortieth Anniversary Meeting, Oct. 7-9, 1977.

Bell, R.E., Karner, G.D. and Steckler, M.S., 1988, Early Mesozoic rift basins of eastern North America and their gravity anomalies: The role of detachments during extension: Tectonics, v.7, p.447-462.

Bonini, W. E. and Woollard, C. P., 1960, Subsurface geology of North Carolina - South Carolina Coastal Plain from seismic data: Bulletin American Association Petroleum Geologists, v.44, p.298-315.

Dallmeyer, R.D., Wright, J.E., Secor, D.T., Jr. and Snoke, A.W., 1986, Character of the Alleghanian orogeny in the Southern Appalachians: Part II. Geochronological constraints on the tectonothermal evolution of the eastern Piedmont in South Carolina: Geological Society of America Bulletin, v.97, p.1329-1344.

Daniels, D.L., 1974, Geologic interpretation of geophysical maps, central Savannah river area, South Carolina and Georgia: U.S. Geological Survey Geophysical Investigations Map GP-893.

Daniels, D.L., Zietz, I. and Popenoe, D., 1983, Distribution of subsurface lower Mesozoic rocks in the Southeastern United States, as interpreted from regional aeromagnetic and gravity maps, *in* Gohn, G.S., ed., Studies Related to the Charleston, South Carolina, Earthquake of 1886 - Tectonics and Seismicity: U.S.G.S. Professional Paper 1313K

Dobrin, M.B., 1960, Introduction to Geophysical Prospecting: New York, McGraw - Hill,

Froelich, A.J.and Olsen, P.E., 1984, Newark Supergroup, A revision of the Newark Group in Eastern North America: U.S. Geological Survey Bulletin, 1537A, p.A55-A58

Guspi, F., and Introcaso, A., 1988, Gravity, its gradients, simultaneous inversion and magnetism - A critical study: Geoexploration, v.25, p.103-112.

Hanson, H.J., 1988, Buried rift basin underlying Coastal Plain sediments, central Delmarva Peninsula, Maryland: Geology, v.16, p.779-782.

Hatcher, R.D., Jr., Howell, D.E. and Talwani, P., 1977, Eastern Piedmont fault system: Speculations on its extent: Geology, v.5, p.636-640.

Maher, H.D., Jr., 1979, Stratigraphy, metamorphism, and structure of the Kiokee and Belair belts near Augusta Georgia [M.S. Thesis]: Columbia, South Carolina, University of South Carolina.

Marine, L.W. and Siple, G.E., 1974, Buried Triassic basin in the central Savannah River area, South Carolina and Georgia: Geological Society of America Bulletin, v.85, p.311-320.

Petty, A. J., Petrafeso, F. A. and Moore, Jr., F. C., 1965, Aeromagnetic Magnetic map of the Savannah River Plant area, South Carolina and Georgia: U. S. Geological Survey Geophysical Investigation Map GP-489.

Secor, D.T., Jr., 1987, Regional Overview. *in* Secor, D.T., Jr., ed, Anatomy of the Alleghanian orogeny as seen from the Piedmont of South Carolina and Georgia: Carolina Geological Society Fieldtrip Guidebook Nov. 14-15, 1987.

Secor, D.T., Jr., Snoke, A.W., Bramlett, K.W., Costello, O.P.and Kimbrell, O.P., 1986, Character of the Alleghanian orogeny in the southern Appalachians: Part I. Alleghanian deformation in the eastern Piedmont of South Carolina: Geological Society of America Bulletin, v.97, p.1319-1328.

Siple, G.E., 1967, Geology and ground water of the Savannah River Plant and vicinity, South Carolina: U.S. Geological Survey Water Supply Paper 1841, p.6.

Speer, J.A., 1982, Description of the Granitoid rocks associated with two gravity minima in Aiken and Barnwell Counties, South Carolina: South Carolina Geology, v.26, p.15-24.

Sumner, J.R., 1977, Geophysical investigation of the structural framework of the Newark - Gettysburg Triassic basin, Pennsylvania: Geological Society of America Bulletin, v.88, p.935-942.

Talwani, P., Long, T. and Bridges, S.R., 1975, Simple Bouger Anomaly Map of South Carolina: MS-21 Division of Geology, South Carolina State Development Board.

Westinghouse Savannah River Co., 1989, Savannah River Site Environmental Report for 1988, WSRC-RP-89-59-1, Volume 1.